Astrocytes close the critical period for visual plasticity

Jérôme Ribot[1‡], Rachel Breton[1,2,3‡#], Charles-Félix Calvo[1], Julien Moulard[1,4], Pascal Ezan[1], Jonathan Zapata[1], Kevin Samama[1], Alexis-Pierre Bemelmans[5], Valentin Sabatet[6], Florent Dingli[6], Damarys Loew[6], Chantal Milleret[1], Pierre Billuart[7], Glenn Dallérac[1£#], Nathalie Rouach[1£*]

[1]Neuroglial Interactions in Cerebral Physiology, Center for Interdisciplinary Research in Biology, Collège de France, CNRS UMR 7241, INSERM U1050, Labex Memolife, PSL Research University Paris, France

[2]Doctoral School N°568, Paris Saclay University, PSL Research University, Le Kremlin Bicetre, France

[3]Astrocytes & Cognition, Paris-Saclay Institute for Neurosciences, CNRS UMR 9197, Paris-Saclay University, Orsay, France

[4]Doctoral School N°158, Sorbonne University, Paris France

[5]Commissariat à l'Energie Atomique et aux Energies Alternatives (CEA), Département de la Recherche Fondamentale, Institut de biologie François Jacob, MIRCen, and CNRS UMR 9199, Université Paris-Saclay, Neurodegenerative Diseases Laboratory, Fontenay-aux-Roses, France

[6]Institut Curie, PSL Research University, Mass Spectrometry and Proteomics Laboratory, Paris, France

[7]Université de Paris, Institute of Psychiatry and Neuroscience of Paris (IPNP), INSERM U1266, Genetic and Development of Cerebral Cortex Laboratory, GHU Paris Psychiatrie et Neurosciences, Hôpital Saint Anne, Paris, France

[‡]Equal contributing authors
[£]Equal contributing authors
[*]Correspondence to: nathalie.rouach@college-de-france.fr
[#]Present address: Astrocytes & Cognition, Paris-Saclay Institute for Neurosciences, CNRS UMR 9197, Paris-Saclay University, Orsay, France

Summary paragraph

Brain postnatal development is characterized by critical periods of experience-dependent remodeling[1,2]. Termination of these periods of intense plasticity is associated with settling of neuronal circuits, allowing for efficient information processing[3]. Failure to end critical periods thus results in neurodevelopmental disorders[4,5]. Yet, the cellular processes defining the timing of these developmental periods remain unclear. Here we show in the mouse visual cortex that astrocytes control the closure of the critical period. We uncover a novel underlying pathway involving regulation of the extracellular matrix that allows interneurons maturation via an unconventional astroglial connexin signaling. We find that timing of the critical period closure is controlled by a marked developmental upregulation of the astroglial protein connexin 30 that inhibits expression of the matrix degrading enzyme MMP9 through the RhoA-GTPase signaling pathway. Our results thus demonstrate that astrocytes not only influence activity and plasticity of single synapses, but are also key elements in the experience-dependent wiring of brain developing circuits. This work, by revealing that astrocytes promote the maturation of inhibitory circuits, hence provide a new cellular target to alleviate malfunctions associated to impaired closure of critical periods.

Main text

During the first weeks of life, massive synaptogenesis occurs and is followed by shaping of synaptic circuits[6]. In the last decades, the role of astroglial processes as structural and signaling partners of individual synapses has been established and their implication in neuronal network activities and cognitive functions has recently been unveiled[7]. Yet, whether they take part in the wiring of the neuronal circuitry that occurs during critical periods of postnatal development remains unknown. The visual cortex is a hallmark brain region of experience-dependent shaping of synaptic circuits during a period of enhanced plasticity that follows eyes opening[2,8]. Intriguingly, one pioneer study published 30 years ago showed that introducing immature astrocytes in adult cats re-opens a period of high plasticity, reminiscent of the critical period[9]. However, since then, whether and how maturation of astrocytes actually take part in the control of the critical periods closure has never been investigated.

Immature astrocytes favor plasticity

We first investigated the ability of immature astrocytes to promote visual cortex plasticity in adult mice. To this end, we cultured and labeled (lentivirus PGK-GFP) immature astrocytes from the cortex of P1-P3 (postnatal day 1-3) mice, and implanted them ten days later in the primary visual cortex (V1) of adult mice (P100), in which the critical period is closed (Fig. 1a). Two weeks after the graft, we tested mice for ocular dominance (OD) plasticity, a form of plasticity typical of the critical period where changes in visual inputs alter the natural dominance of the contralateral eye. To do so, we assessed visual cortex activity using optical imaging of intrinsic signals after four days of monocular deprivation (MD) (Fig. 1a). We found that mice engrafted with immature astrocytes displayed a high level of plasticity, unlike control mice subjected to MD with injection of culture medium or non-injected mice (Fig. 1b-c). These data indicate that immature astrocytes re-open OD plasticity in adult mice.

To identify how immature astrocytes favor OD plasticity, we then investigated the molecular determinants of astroglial maturation. Comparing gene expression of immature (P7) *vs* mature

(P30) astrocytes using the transcriptome database for astrocytes during development[10] revealed about 200 genes that were differentially expressed with a fold-change over 5 (Extended data Table 1). Gene Ontology analysis of enriched astroglial gene groups identified a functional switch during maturation from cell division to cell communication, with the cell junction genes being the most represented (Extended Table 2 and Fig. 1). Among these genes, *Gjb6*, encoding the astroglial gap-junction channel subunit connexin 30 (Cx30), displayed one of the highest increase in expression (Fold-change=9, P=0.0274; Extended Data Table 1). Accordingly, we recently found that Cx30 regulates the structural maturation of hippocampal astrocytes during postnatal development[11]. Together, these data incited us to investigate the role of Cx30 in the astroglial control of the critical period. To do so, we first assessed the regional and temporal expression of Cx30 in the mouse V1. We found by immunohistochemistry that Cx30 is enriched in layer 4, the main V1 input layer, identified by Wisteria Floribunda Agglutinin (WFA), a marker of perineuronal nets important for the timecourse of the critical period[12]. This enrichment correlates with a high density of astrocytes labeled in the Aldh1l1-gfp mice (Fig. 1d). Moreover, Cx30 protein levels increased from P10 to P50, as shown by western blot (Fig. 1e), reaching its maximum when the critical period ends, thus suggesting that it may contribute to its closure. If so, re-opening a phase of high plasticity should be associated with a downregulation of Cx30. As a period of dark exposure (DE) can reinstate visual cortex plasticity during adulthood after closure of the critical period[13,14], we placed wild-type adult mice (P50) in the dark for 4 days and quantified V1 Cx30 levels. We found that this manipulation drastically reduced Cx30 protein levels (~-70%) (Fig. 1f). Remarkably, we also found that the same DE for 4 days induced by itself V1 plasticity, as indicated by the change in OD index, which suggests that astroglial Cx30 is a brake to plasticity (Fig. 1g-h).

Astroglial Cx30 closes the critical period

We then directly investigated whether Cx30 inhibits OD plasticity. To do so, we first generated an astroglial knockdown mouse line for Cx30 (KD), where Cx30 expression is decreased in V1 astrocytes by ~70% (Extended data Fig. 2). In these mice, electroretinograms were unaltered, suggesting normal retinal functions (Extended Fig. 3). We found that OD plasticity peaked at P28 in wild-type (WT) mice. In contrast, this plasticity continued to increase in KD mice until P50, indicating an impairment in the closure of the critical period (Fig. 2a, b). While in WT mice this plasticity was due to an increase in the open eye response, in KD mice, it resulted from a reduction of the closed eye response, which typically reflects changes occurring in mature and immature system, respectively[15]. These data thus indicate that Cx30 is required for proper maturation of the visual cortex.

To further directly test that the expression of Cx30 in mature astrocytes inhibits OD plasticity, we engrafted mature astrocytes expressing or not Cx30, isolated from P19 wild type or constitutive Cx30 knockout mice, respectively (Fig. 2d, e). By doing so, we found that only the graft of mature astrocytes lacking Cx30 re-opened OD plasticity in adult mice (Fig. 2f). Altogether, these data indicate that astroglial Cx30 controls the timing of the critical period closure.

Astroglial Cx30 promotes the maturation of inhibitory circuits

The temporal course of visual cortex critical period is determined by the maturation of local inhibitory circuits controlling the excitation-inhibition (E-I) balance[16-18]. To get insights on the physiological processes via which Cx30 closes the critical period, we thus measured changes in excitatory and inhibitory synaptic transmission following MD in pyramidal neurons from layer 4 visual cortex of WT and KD adult mice (P50) (Fig. 3a). The frequency, but not the amplitude, of both spontaneous excitatory and inhibitory postsynaptic currents (sEPSCs and sIPSCs) were markedly reduced in KD mice compared to WT (Fig. 3b-c). In addition, MD induced an increase in the frequency of sEPSC and sIPSCs in KD mice while it had no effect in WT, indicating that experience-dependent plasticity of both excitatory and inhibitory synapses occurs in adult KD, but not in WT mice. As excitation and inhibition influence each other through homeostatic processes[19], we then assessed whether the E-I balance was affected by analyzing the dynamic conductances of evoked composite synaptic responses. We found the inhibition/excitation ratio to be reduced in KD mice (Fig. 3d-e), thus indicating functionally that inhibition is primarily affected by Cx30 downregulation. Further, as found for the sEPSC/sIPSC data, I-E ratio increased when plasticity was induced through MD. Together, these data suggest that experience-dependent maturation of inhibitory circuits ending the critical period requires astroglial Cx30. To investigate this possibility, we assessed maturity of PV interneurons, which settle visual cortex inhibition, by determining the abundance of their perineuronal nets (PNN) of extracellular matrix (ECM) proteins[12]. We found PNN to be significantly smaller in KD mice (Fig. 3f-g), thus revealing the immaturity of these cells. In addition, while MD also decreased PNN in WT mice, it had no further effect in KD mice, suggesting that reduction of PNN is a prerequisite for plasticity. Together, these data indicate that the developmental rise of Cx30 during the critical period is required for the timely maturation of visual cortex inhibition.

Astroglial Cx30 closes the critical period by downregulating the RhoA-MMP9 pathway

We then sought to identify the molecular pathway through which Cx30 modulates PNN extent and maturation of PV interneurons. To this end we performed co-immunoprecipitation experiments with biotinylated WFA lectin followed by quantitative proteomics of pulled down proteins in WT and KD mice using label-free mass spectrometry. Reactome pathway analysis of enriched or unique proteins in WT compared to KD samples indicated an enrichment of proteins associated with the Rho GTPases-KTN1 pathway (Extended data Table 3, Fig. 4a upper panel). Conversely, analysis of proteins unique and enriched in KD compared to WT samples revealed enrichment of the RhoGTPases-ROCK pathway (Extended data Table 3, Fig. 4a). Besides, mass spectrometry analysis of Cx30 co-immunoprecipitates indicated interactions with Rho-GTPases signaling pathways, among which the Rho-associated protein kinase ROCK2 was significantly enriched in KD compared to WT (Extended data Table 4, Fig. 4a lower panel). Together, this exploratory approach points to a role of the Rho family of GTPases in the PNN changes between WT and KD mice.

RhoA, one family member of the Rho-GTPases, plays a key role in cell remodeling[20] through activation of ROCKs and its interactions with different connexins has been described in other cell types[21,22]. We thus tested the activation of RhoA by assessing levels of RhoA-GTP using immunohistochemistry, and found a strong increase in KD mice (Fig. 4b). In addition, while

MD also increased RhoA-GTP in WT mice, it had no further effect in KD mice, suggesting that activation of RhoA pathway is a prerequisite for plasticity.

As the RhoA-ROCK pathway can modulate the expression of the ECM degrading enzyme Matrix Metalloproteinase-9 (MMP9)[23,24], we next tested whether this signaling is involved in the Cx30 regulation of PNNs and PV interneurons maturation. To do so, we assessed MMP9 expression in layer 4 of the visual cortex, and found that MMP9 levels were markedly increased in KD mice compared to WT mice (Fig. 4c). In addition, akin to RhoA-GTP, while MD increased MMP9 levels in WT mice, it had no additional effect in KD mice (Fig. 4c). This suggests that activation of the RhoA-ROCK pathway leads to the degradation of PNNs through MMP9 in both KD mice and WT mice under MD condition. We next directly tested this hypothesis by inhibiting the ROCK signaling pathway in vivo with fasudil (Fig. 4d) and found that it rescued both MMP9 levels and PNN extent in KD mice, while it had no effect in WT mice (Fig. 4e, f). These data therefore indicate that astroglial Cx30 regulates MMP9 levels and PV cell maturation via the RhoA-ROCK signaling pathway.

Discussion

We here demonstrate that astrocytes control timing for closure of the postnatal critical period of experience-dependent remodeling. We further identify that they achieve this through developmental rise of the astroglial protein Cx30, which we found to inhibit expression of MMP9 via the RhoA-ROCK pathway, thereby hindering maturation of local inhibition. While the latter is established as a trigger for critical period closure, its control by astroglial signaling place astrocytes as key elements orchestrating the shaping of synaptic circuits. Beyond its role in critical period, the identified pathway may well be involved in structural synaptic plasticity associated with cognitive functions, since we previously found that Cx30 regulates the structure and efficacy of the tripartite synapse in the hippocampus[25]. The regulation of MMP9 levels that we here describe occurs via an unconventional signaling through Cx30 and thus represents a novel astroglial pathway regulating wiring of brain circuits. Because extended critical periods are associated with neurodevelopmental defects resulting in sensori-motor or psychiatric disorders[4,5], these findings provide a new target for the development of strategies aiming at re-inducing a period of enhanced plasticity in adults and favor rehabilitation after brain damage or developmental malfunction.

References

1 Espinosa, J. S. & Stryker, M. P. Development and plasticity of the primary visual cortex. *Neuron* **75**, 230-249, doi:10.1016/j.neuron.2012.06.009 (2012).

2 Hubel, D. H. & Wiesel, T. N. The period of susceptibility to the physiological effects of unilateral eye closure in kittens. *J Physiol* **206**, 419-436, doi:10.1113/jphysiol.1970.sp009022 (1970).

3 Hensch, T. K. Critical period regulation. *Annu Rev Neurosci* **27**, 549-579, doi:10.1146/annurev.neuro.27.070203.144327 (2004).

4 LeBlanc, J. J. & Fagiolini, M. Autism: a "critical period" disorder? *Neural Plast* **2011**, 921680, doi:10.1155/2011/921680 (2011).

5 Meredith, R. M. Sensitive and critical periods during neurotypical and aberrant neurodevelopment: a framework for neurodevelopmental disorders. *Neurosci Biobehav Rev* **50**, 180-188, doi:10.1016/j.neubiorev.2014.12.001 (2015).

6 Doll, C. A. & Broadie, K. Impaired activity-dependent neural circuit assembly and refinement in autism spectrum disorder genetic models. *Front Cell Neurosci* **8**, 30, doi:10.3389/fncel.2014.00030 (2014).

7 Clarke, L. E. & Barres, B. A. Emerging roles of astrocytes in neural circuit development. *Nat Rev Neurosci* **14**, 311-321, doi:10.1038/nrn3484 (2013).

8 Lehmann, K. & Lowel, S. Age-dependent ocular dominance plasticity in adult mice. *PLoS One* **3**, e3120, doi:10.1371/journal.pone.0003120 (2008).

9 Muller, C. M. & Best, J. Ocular dominance plasticity in adult cat visual cortex after transplantation of cultured astrocytes. *Nature* **342**, 427-430, doi:10.1038/342427a0 (1989).

10 Cahoy, J. D. *et al.* A transcriptome database for astrocytes, neurons, and oligodendrocytes: a new resource for understanding brain development and function. *J Neurosci* **28**, 264-278, doi:10.1523/JNEUROSCI.4178-07.2008 (2008).

11 Ghezali, G. *et al.* Connexin 30 controls astroglial polarization during postnatal brain development. *Development* **145**, doi:10.1242/dev.155275 (2018).

12 Pizzorusso, T. *et al.* Reactivation of ocular dominance plasticity in the adult visual cortex. *Science* **298**, 1248-1251, doi:10.1126/science.1072699 (2002).

13 Erchova, I., Vasalauskaite, A., Longo, V. & Sengpiel, F. Enhancement of visual cortex plasticity by dark exposure. *Philos Trans R Soc Lond B Biol Sci* **372**, doi:10.1098/rstb.2016.0159 (2017).

14 He, H. Y., Ray, B., Dennis, K. & Quinlan, E. M. Experience-dependent recovery of vision following chronic deprivation amblyopia. *Nat Neurosci* **10**, 1134-1136, doi:10.1038/nn1965 (2007).

15 Hofer, S. B., Mrsic-Flogel, T. D., Bonhoeffer, T. & Hubener, M. Lifelong learning: ocular dominance plasticity in mouse visual cortex. *Curr Opin Neurobiol* **16**, 451-459, doi:10.1016/j.conb.2006.06.007 (2006).

16 Di Cristo, G. *et al.* Activity-dependent PSA expression regulates inhibitory maturation and onset of critical period plasticity. *Nat Neurosci* **10**, 1569-1577, doi:10.1038/nn2008 (2007).

17 Hensch, T. K. *et al.* Local GABA circuit control of experience-dependent plasticity in developing visual cortex. *Science* **282**, 1504-1508, doi:10.1126/science.282.5393.1504 (1998).

18 Tropea, D. *et al.* Gene expression changes and molecular pathways mediating activity-dependent plasticity in visual cortex. *Nat Neurosci* **9**, 660-668, doi:10.1038/nn1689 (2006).

19 Turrigiano, G. G. & Nelson, S. B. Homeostatic plasticity in the developing nervous system. *Nat Rev Neurosci* **5**, 97-107, doi:10.1038/nrn1327 (2004).

20 Gonzalez-Billault, C. *et al.* The role of small GTPases in neuronal morphogenesis and polarity. *Cytoskeleton (Hoboken)* **69**, 464-485, doi:10.1002/cm.21034 (2012).

21 Kim, H. J. *et al.* RhoA/ROCK Regulates Prion Pathogenesis by Controlling Connexin 43 Activity. *Int J Mol Sci* **21**, doi:10.3390/ijms21041255 (2020).

22 Mendoza-Naranjo, A. *et al.* Targeting Cx43 and N-cadherin, which are abnormally upregulated in venous leg ulcers, influences migration, adhesion and activation of Rho GTPases. *PLoS One* **7**, e37374, doi:10.1371/journal.pone.0037374 (2012).

23 Jeong, K. J. *et al.* The Rho/ROCK pathway for lysophosphatidic acid-induced proteolytic enzyme expression and ovarian cancer cell invasion. *Oncogene* **31**, 4279-4289, doi:10.1038/onc.2011.595 (2012).

24 Tong, L. & Tergaonkar, V. Rho protein GTPases and their interactions with NFkappaB: crossroads of inflammation and matrix biology. *Biosci Rep* **34**, doi:10.1042/BSR20140021 (2014).

25 Pannasch, U. *et al.* Connexin 30 sets synaptic strength by controlling astroglial synapse invasion. *Nat Neurosci* **17**, 549-558, doi:10.1038/nn.3662 (2014).

Acknowledgments

This work was supported by grants from the European Research Council (Consolidator grant #683154), European Union's Horizon 2020 research and innovation program (Marie Sklodowska-Curie Innovative Training Networks, grant #722053, EU-GliaPhD) and UNADEV-Aviesan to N.R., from Région Ile-de-France and Fondation pour la Recherche Médicale to D.L., from College de France to G.D., from Fyssen Fondation to J.Z. and from French Research Ministry (Biosigne Doctoral school) to R.B. The authors thank Noëlle Dufour, Charlène Joséphine and MIRCen's viral vector facility, the animal and imaging facilities of College de France as well as Michel Roux from the mouse clinical institute for excellent technical assistance.

Author Contributions

Conceptualization: N.R., G.D., J.R. C.M.; Data curation: G.D., J.R., R.B. D.L., N.R.; Formal analysis: G.D., J.R., R.B., P.B., J.Z., V.S., D,L., N.R.; Funding acquisition: N.R., G.D.; Investigation: J.R., R.B., G.D., C.F.C., F.D., P.E., K.S., J. Z., N.R.; Methodology: J.R., G.D., J.M.; Resources: D.L., A.P.B.; Supervision: N.R., G.D.; Project administration: N.R.; Validation: J.R., G.D., N.R.; Visualization: J.R., R.B., G.D., N.R.; Writing original draft: G.D., N.R.; Writing – review & editing: all authors.

Competing interests

The authors declare no competing interests.

Additional Information

Supplementary Information is available for this paper.

Correspondence and requests for materials should be addressed to N.R.

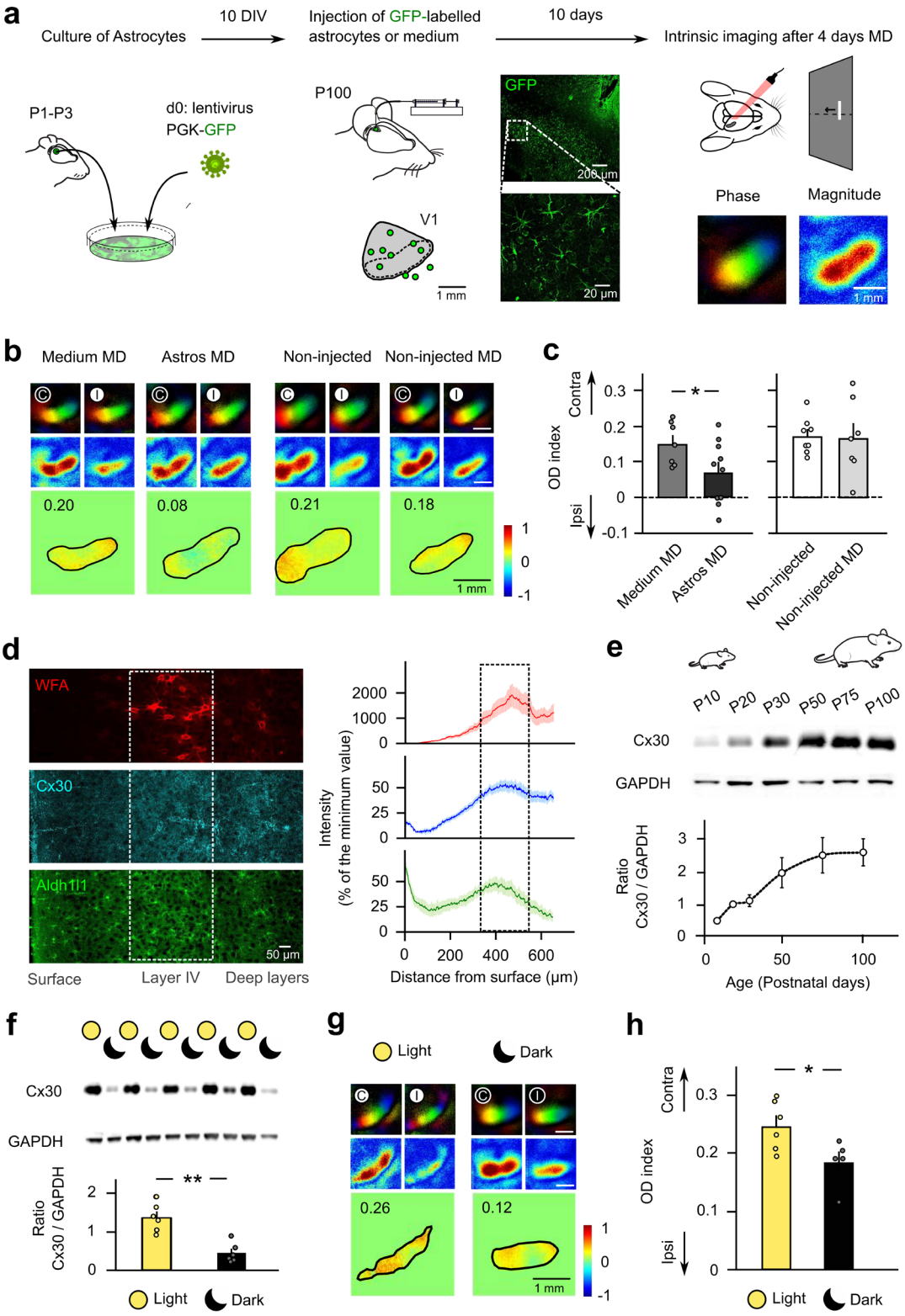

Figure 1. Immature astrocytes favor cortical plasticity. (a) Immature astrocytes from P1-P3 mice were transduced with PGK-GFP lentivirus, cultured for 10 DIV, and injected in the V1 area of adult mice (P100), as shown on the schematic (green circles), where the dashed line represents the binocular zone. Confocal images of GFP-expressing astrocytes integrated in the visual cortex of injected mice are shown. Intrinsic optical imaging was then conducted to record phase and magnitude retinotopic maps for each eye stimulation after 4 days of monocular deprivation (MD). (b) These maps are shown in top panels for animals injected

with control medium (Medium MD, n=7) or immature astrocytes (Astro MD, n=10) and for non-injected mice in control (non-injected, n=8) or MD (non-injected MD, n=7) conditions. Stimulated contralateral (C) and ipsilateral (I) eyes are indicated with a white (open) or black (closed) circle. Bottom panels show the normalized OD map with average value inset. (c) Mice injected with immature astrocytes showed a marked increase in OD plasticity compared with control mice injected with culture medium (P=0.043, DF=15, two-tailed t-test), while no effect was observed in non-injected mice (P=0.899, DF=13, two-tailed t-test). (d) Representative immunostaining for WFA (top), Cx30 (middle) and Aldh1l1 (bottom) in V1 of P50 mouse (left panels), and corresponding quantification of spatial distributions across V1 layers (right panels, n=3 mice). (e) Western blot analysis reveals changes in Cx30 levels in the visual cortex during development (n=6 per age, P=0.0001, Kruskal-Wallis (KW=22.31)) and (f) after 4 days of dark exposure (n=6 per group, P=0.0022, U=0, Mann-Whitney test). (g) Intrinsic optical imaging for light (n=6) and dark (n=5) exposed animals showing that (h) dark exposure decreased OD index (P=0.035, DF=9, two-tailed t-test).

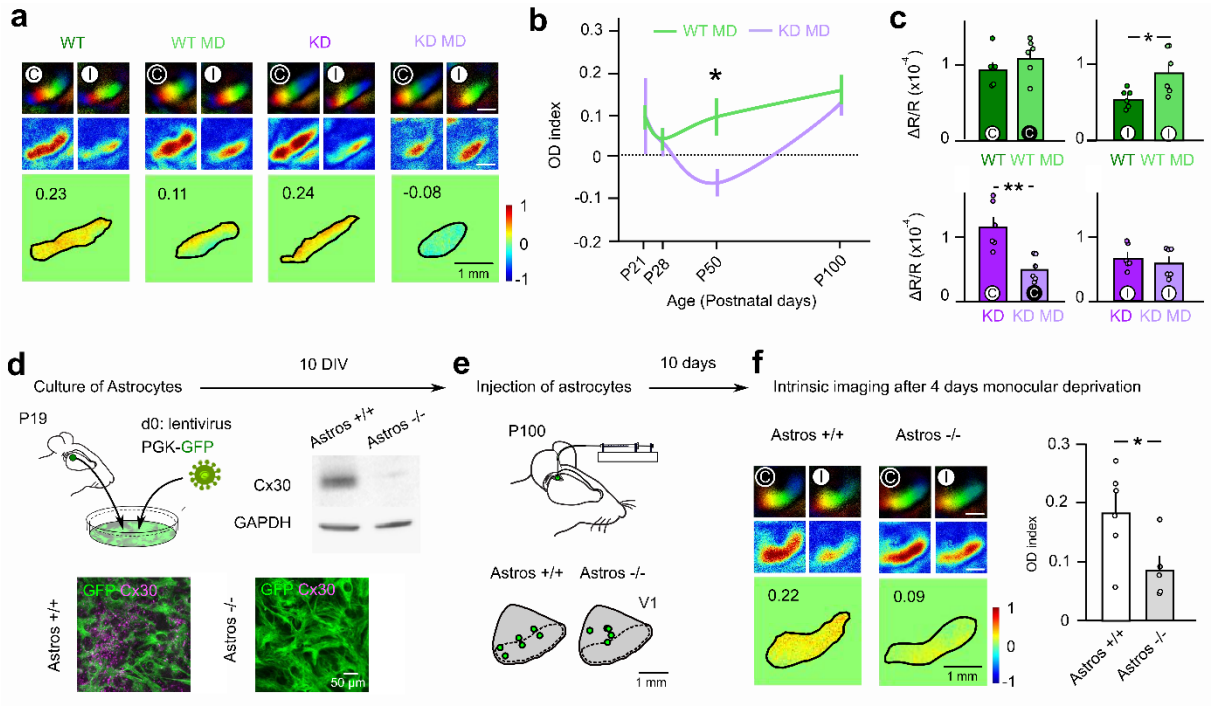

Figure 2. Astroglial connexin 30 closes the critical period. (a) Functional maps in P50 wild-type (WT) and Cx30 knockdown (KD) mice in control and MD conditions. (b) Developmental profile of OD index after MD in WT (P21, n=6; P28, n=7; P50, n=6; P100, n=7) and KD mice (P21, n=3; P28, n=8; P50, n=6; P100, n=11), indicating a protracted and enhanced plasticity at P50 in KD mice (P=0.0232, DF=46, two-way ANOVA followed by Sidak post-hoc test). (c) Changes in response magnitude after MD in P50 mice result from an increased response to the open (ipsilateral, I) eye stimulation in WT mice (n=6, P=0.0411, U=5, Mann Whitney test), and from a decreased response to the closed (contralateral, C) eye stimulation in KD mice (n=6, P=0.0022, U=0, Mann-Whitney test). (d) Mature astrocytes expressing or not Cx30 were isolated from P19 WT (Astro +/+) or constitutive Cx30 knockout mice (Astros -/-), respectively, and were then transduced with PGK-GFP lentiviruses and cultured for 10 DIV. Western blots and immunostaining show expression of Cx30 in Astro +/+, but not in Astro -/-. (e) The cultured astrocytes were injected in adult mice (P100), as shown on the schematics (green circles). (f) Functional maps show that OD plasticity is enhanced in mice injected with Astro -/- (n=5) compared to mice injected with Astro +/+ (n=6, P=0.038, DF=9, two-tailed t-test).

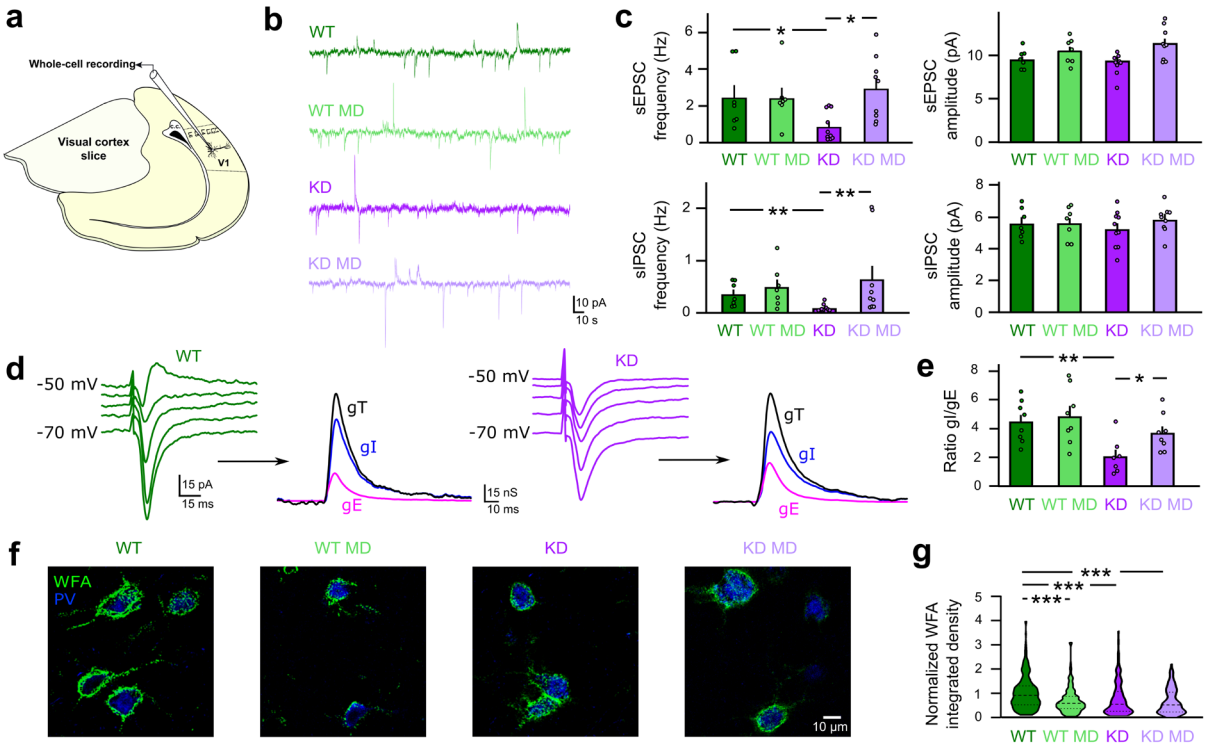

Figure 3. Astroglial Cx30 promotes the maturation of inhibitory circuits. (a) Schematic diagram depicting the brain slice from which V1 pyramidal neurons from layer 4 were recorded. (b) Example traces of sEPSCs (inward) and sIPSCs (outward) currents. (c) Frequency, but not amplitude, of both sEPSCs (P=0.0192, U=11, Mann-Whitney test) and sIPSCs (P=0.0034, U=5, Mann-Whitney test) was decreased in KD (n=10) compared to WT mice (n=7). MD induced no plasticity in WT mice (n=7, P=0.7027, U=19 for sEPSCs, P=0.6547 U=21, for sIPSCs, Mann-Whitney test), while it potentiated both the sEPSCs (P=0.0090, U=13, Mann-Whitney test) and sIPSCs (P=0.0019, U=13, Mann-Whitney test) in KD mice (n=9). (d) Example of evoked composite responses at increasing holding potentials allowing decomposition of the total conductance (gT) into excitatory (gE) and inhibitory (gI) conductances in WT and KD mice. (e) Inhibition/Excitation (I/E) ratio was reduced in KD mice (n=7, P=0.0078, U=5, Mann-Whitney test) compared to WT (n=8). MD induced no change in WT mice (n=8, P=0.7527, U=29, Mann-Whitney test), while it increased the I/E ratio in KD mice (n=8, P=0.020, U=8, Mann-Whitney test). (f) WFA immunostaining and (g) violin plot showing smaller perineuronal nets around PV interneurons in KD (n=177 cells from 16 mice, P<0.0001), WT MD (n=171 cells from 6 mice, P=0.0007) and KD MD mice (n=133 cells from 3 mice, p<0.0001) compared to WT mice (n=226 cells from 16 mice) (Kruskal-Wallis (KW= 45.64) followed by Dunn's multiple comparisons post-hoc).

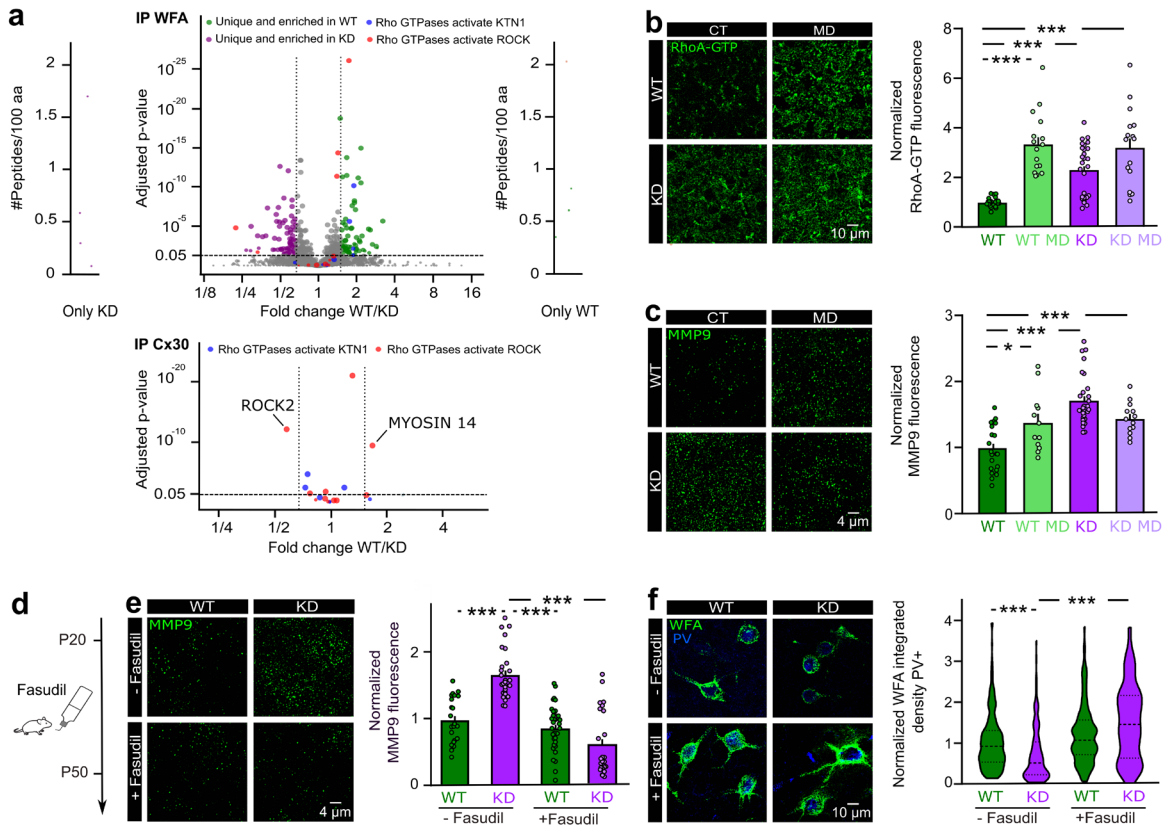

Figure 4. Astroglial Cx30 downregulates the RhoA-MMP9 pathway. (a) Top, volcano plot analysis representing the 2096 quantified proteins with at least 3 total peptides in all replicates enriched with biotinylated WFA lectin in KD and WT mice. Binding partners were obtained by using quantitative label-free mass spectrometry analysis performed from three replicates. Dashed vertical lines denote absolute fold change of 1.5 and the dashed horizontal line denotes the adjusted P-value of ratio significance of 0.05. Selected enriched proteins in WT (green) and KD (purple) samples are shown. Proteins from the enriched pathways Rho-GTPase activate KTN1 (blue) and Rho-GTPase activate ROCK (red) are highlighted. External plots show proteins with peptides identified only in one sample type (left in KD and right in WT). Bottom, volcano plot analysis representing interactors of Cx30 from the Rho-GTPase activate KTN1 (blue) and Rho-GTPase activate ROCK (red) pathways. The fold-change in WT (n=5) versus KD mice (n=4) are shown with selected proteins (Rock2 and Myosin 14) quantified with an absolute fold change ≥ 1.5, an adjusted P-value ≤ 0.05 and with ≥ 3 peptides. (b) Immunostaining for RhoA-GTP showed a marked increase in KD (n=27, P=0.0003), KD MD (n=16, P<0.0001) and WT MD mice (n=16, P<0.0001) compared to WT mice (n=22) (slices from 3 mice per group) (Kruskal-Wallis (KW=41.23) followed by Dunn's post-hoc test. (c) Immunostaining for MMP9 shows a marked increase in KD mice (n=28, P<0.0001, DF=71), KD MD (n=13, P=0.0059, DF=71) and MD mice (n=12, P=0.0322, DF=71) compared to WT mice (n=22) (ANOVA (F(3,71)=15.07) followed by Tukey's post-hoc test). (d) Diagram depicting the protocol for experimental treatment with Fasudil. (e) Fasudil rescued MMP9 levels in KD mice (KD+Fasudil: n=25 from 5 mice, KD=28 slices from 3 mice, P<0.0001), while it had no effect in WT mice (WT+Fasudil: n=34 from 6 mice, WT: 22 slices from 3 mice, P>0.9999, Kruskall-Wallis (KW=55.98) followed by Dunn's post-hoc test). (f) Fasudil rescued perineuronal nets levels in KD mice (KD+Fasudil:

n=52 from 5 mice; KD, n=177 from 16 mice, P<0.0001) while it had no effect in WT mice (WT+Fasudil, n=129 from 6 mice, WT, n=226 from 16 mice, P=0.1510) (Kruskall-Wallis (KW=71.65) followed by Dunn's post-hoc test).

Extended Data for

Astrocytes close the critical period for visual plasticity

Jérôme Ribot[1‡], Rachel Breton[1,2‡#], Charles-Félix Calvo[1], Julien Moulard[1], Pascal Ezan[1], Jonathan Zapata[1], Kevin Samama[1], Alexis-Pierre Bemelmans[3], Valentin Sabatet[4], Florent Dingli[4], Damarys Loew[4], Chantal Milleret[1], Pierre Billuart[5], Glenn Dallérac[1£#], Nathalie Rouach[1£*]

[*]Correspondence to: nathalie.rouach@college-de-france.fr

This PDF file includes:

Extended Data Figures 1-3

Tables 1-4

Probe ID	Gene,symbol	Gene,title	adj,P,Val	Fold-Change in mature over immature astrocytes
Enriched genes				
1441430_at	cDNA1	UI-M-DJ2-bwb-i-13-0-UI.s1 NIH_BMAP_DJ2 Mus musculus cDN/	0.0185	111.4304721
1452975_at	Etnppl	ethanolamine phosphate phospholyase	0.019	78.24897777
1433785_at	Mobp	myelin-associated oligodendrocytic basic protein	0.019	34.2967508
1443745_s_at	Dmp1	dentin matrix protein 1	0.019	28.4429658
1421425_a_at	Rcan2	regulator of calcineurin 2	0.019	24.08394796
1455913_x_at	Ttr	transthyretin	0.019	19.56224444
1419300_at	Flt1	FMS-like tyrosine kinase 1	0.0222	18.50701094
1417185_at	Ly6a	lymphocyte antigen 6 complex, locus A	0.019	16.56423878
1418091_at	Tfcp2l1	transcription factor CP2-like 1	0.019	16.1112888
1427345_a_at	Sult1a1	sulfotransferase family 1A, phenol-preferring, member 1	0.019	15.45498126
1417852_x_at	Clca3a1	chloride channel accessory 3A1	0.0214	15.24220797
1456228_x_at	Mbp	myelin basic protein	0.019	14.92852786
1427183_at	Efemp1	epidermal growth factor-containing fibulin-like extracellular n	0.0246	13.08643294
1435918_at	Fam107a	family with sequence similarity 107, member A	0.019	12.38051995
1450468_at	Myoc	myocilin	0.0227	10.55606329
1435851_at	Lgi1	leucine-rich repeat LGI family, member 1	0.019	10.41073484
1440225_at	Adgrf5	adhesion G protein-coupled receptor F5	0.0227	10.056107
1429166_s_at	Clmn	calmin	0.019	9.9176616
1457495_at	2900052N01Rik	RIKEN cDNA 2900052N01 gene	0.0214	9.781122222
1457373_at	Cdh19	cadherin 19, type 2	0.0251	9.646462622
1459570_at	Gpr143	G-protein–coupled receptor 143	0.0232	9.382679594
1439668_at	Gm11681	predicted gene 11681	0.019	9.18958684
1456633_at	Trpm3	transient receptor potential cation channel, subfamily M, meml	0.0236	9.126109727
1448397_at	Gjb6	gap junction protein, beta 6	0.0274	9.063071082
1429177_x_at	Sox17	SRY (sex determining region Y)-box 17	0.0199	8.75434961
1416468_at	Aldh1a1	aldehyde dehydrogenase family 1, subfamily A1	0.0251	8.633825892
1424854_at	Hist1h4m///Hist1h4	histone cluster 1, H4m///histone cluster 1, H4b///histone cluste	0.019	8
1451580_a_at	Ttr	transthyretin	0.019	8
1452318_a_at	Hspa1b	heat shock protein 1B	0.019	7.835362381
1459197_at	Cntn1	contactin 1	0.0199	7.781239579
1437056_x_at	Crispld2	cysteine-rich secretory protein LCCL domain containing 2	0.019	7.781239579
1436698_x_at	Tmem204	transmembrane protein 204	0.019	7.727490631
1425506_at	Mylk	myosin, light polypeptide kinase	0.019	7.568461174
1419759_at	Abcb1a	ATP-binding cassette, sub-family B (MDR/TAP), member 1A	0.0199	7.464263932
1417574_at	Cxcl12	chemokine (C-X-C motif) ligand 12	0.0246	7.412704495
1445565_at	Hist1h2bg///Hist1h2	histone cluster 1, H2bg///histone cluster 1, H2be///histone clus	0.019	7.160200567
1435741_at	Pde8b	phosphodiesterase 8B	0.019	7.160200567
1424553_at	Hhatl	hedgehog acyltransferase-like	0.019	7.110741449
1445961_at	cDNA5	H3101D08-3 NIA Mouse 15K cDNA Clone Set Mus musculus cDN	0.019	7.110741449
1460259_s_at	Clca3a2///Clca3a1	chloride channel accessory 3A2///chloride channel accessory 3	0.0199	7.012845771
1422155_at	Hist2h3b///Hist1h3e	histone cluster 2, H3b///histone cluster 1, H3e///histone cluster	0.019	6.91629785
1436386_x_at	Zfp982	zinc finger protein 982	0.03	6.821079134
1428387_at	Acsl3	acyl-CoA synthetase long-chain family member 3	0.019	6.773962499
1427126_at	Hspa1b	heat shock protein 1B	0.019	6.727171322
1436367_at	Ptprb	protein tyrosine phosphatase, receptor type, B	0.0203	6.680703355
1454969_at	Lypd6	LY6/PLAUR domain containing 6	0.019	6.634556367
1437264_at	BC051142	cDNA sequence BC051142	0.019	6.453134074
1458379_at	9330159F19Rik	RIKEN cDNA 9330159F19 gene	0.027	6.453134074
1452385_at	Usp53	ubiquitin specific peptidase 53	0.019	6.408559021
1416239_at	Gm5424///Ass1	argininosuccinate synthase pseudogene///argininosuccinate syr	0.0267	6.276672783
1428394_at	Lrrc8a///Phyhd1	leucine rich repeat containing 8A///phytanoyl-CoA dioxygenas	0.019	6.233316637
1455452_x_at	Kctd14	potassium channel tetramerisation domain containing 14	0.0359	6.105036836
1459223_at	B930095G15Rik	RIKEN cDNA B930095G15 gene	0.0214	6.105036836
1434628_a_at	Rhpn2	rhophilin, Rho GTPase binding protein 2	0.019	6.062866266
1419383_at	S100b	S100 protein, beta polypeptide, neural	0.0201	6.02098699
1425537_at	Ppm1a	protein phosphatase 1A, magnesium dependent, alpha isoform	0.019	5.979396995
1460043_at	cDNA2	BB357628 RIKEN full-length enriched, adult male corpus striatum I	0.0251	5.897076869
1439096_at	Ddo	D-aspartate oxidase	0.0221	5.856342784
1418788_at	Tek	endothelial-specific receptor tyrosine kinase	0.0191	5.856342784
1436569_at	Prex2	phosphatidylinositol-3,4,5-trisphosphate-dependent Rac excha	0.0229	5.856342784
1424842_a_at	Arhgap24	Rho GTPase activating protein 24	0.0191	5.815890069
1459849_x_at	Vcpip1	valosin containing protein (p97)/p47 complex interacting prote	0.019	5.815890069
1439830_at	Map3k5	mitogen-activated protein kinase kinase kinase 5	0.0232	5.775716782
1425811_a_at	Csrp1	cysteine and glycine-rich protein 1	0.0262	5.735820992

1449102_at	Ebf2	early B cell factor 2	0.0277	5.656854249
1416069_at	Pfkp	phosphofructokinase, platelet	0.0191	5.656854249
1435640_x_at	A130040M12Rik	RIKEN cDNA A130040M12 gene	0.0881	5.656854249
1423523_at	Aass	aminoadipate-semialdehyde synthase	0.027	5.578974665
1436173_at	Dlc1	deleted in liver cancer 1	0.0236	5.578974665
1439655_at	cDNA3	H3018G09-3 NIA Mouse 15K cDNA Clone Set Mus musculus cDN	0.0231	5.578974665
1434354_at	Maob	monoamine oxidase B	0.0199	5.464161027
1435361_at	Sema3g	sema domain, immunoglobulin domain (Ig), short basic domai	0.019	5.464161027
1416164_at	Fbln5	fibulin 5	0.0237	5.42641731
1416200_at	Il33	interleukin 33	0.0251	5.388934307
1448961_at	Plscr2	phospholipid scramblase 2	0.0464	5.388934307
1450653_at	Spz1	spermatogenic leucine zipper 1	0.0191	5.388934307
1437277_x_at	Tgm2	transglutaminase 2, C polypeptide	0.0204	5.388934307
1438287_x_at	Ddx39	DEAD (Asp-Glu-Ala-Asp) box polypeptide 39	0.0878	5.351710219
1455799_at	Rorb	RAR-related orphan receptor beta	0.0191	5.314743256
1438980_x_at	Pm20d1	peptidase M20 domain containing 1	0.024	5.278031643
1416003_at	Cldn11	claudin 11	0.025	5.241573615
1447854_s_at	Hist2h2be	histone cluster 2, H2be	0.0199	5.241573615

Downregulated genes

1451246_s_at	Aurkb	aurora kinase B	0.019	-51.26847217
1454694_a_at	Top2a	topoisomerase (DNA) II alpha	0.019	-24.42014734
1439904_at	Fstl5	follistatin-like 5	0.019	-20.39297004
1448314_at	Cdk1	cyclin-dependent kinase 1	0.019	-16.1112888
1448627_s_at	Pbk	PDZ binding kinase	0.019	-15.24220797
1434819_at	St6gal2	beta galactoside alpha 2,6 sialyltransferase 2	0.019	-14.32040113
1436847_s_at	Cdca8	cell division cycle associated 8	0.019	-14.2214829
1416558_at	Melk	maternal embryonic leucine zipper kinase	0.019	-13.8325957
1426817_at	Mki67	antigen identified by monoclonal antibody Ki 67	0.019	-12.81711804
1423775_s_at	Prc1	protein regulator of cytokinesis 1	0.019	-11.79415374
1420994_at	B3gnt5	UDP-GlcNAc:betaGal beta-1,3-N-acetylglucosaminyltransfer	0.019	-11.79415374
1419153_at	2810417H13Rik	RIKEN cDNA 2810417H13 gene	0.019	-11.15794933
1428304_at	Esco2	establishment of sister chromatid cohesion N-acetyltransferase	0.0277	-10.48314723
1436013_at	Gsg1l	GSG1-like	0.019	-10.48314723
1417458_s_at	Cks2	CDC28 protein kinase regulatory subunit 2	0.019	-10.056107
1417910_at	Ccna2	cyclin A2	0.019	-9.9176616
1447363_s_at	Bub1b	BUB1B, mitotic checkpoint serine/threonine kinase	0.019	-9.781122222
1429295_s_at	Trip13	thyroid hormone receptor interactor 13	0.019	-9.781122222
1430000_at	B230117O15Rik	RIKEN cDNA B230117O15 gene	0.0506	-9.579829637
1452954_at	Ube2c	ubiquitin-conjugating enzyme E2C	0.019	-9.579829637
1416251_at	Mcm6	minichromosome maintenance complex component 6	0.019	-9.382679594
1438262_at	Slc8a2	solute carrier family 8 (sodium/calcium exchanger), member 2	0.019	-9.000467878
1436808_x_at	Mcm5	minichromosome maintenance complex component 5	0.019	-8.815240927
1456231_at	Pla2g3	phospholipase A2, group III	0.0227	-8.339726087
1460627_at	Thsd7b	thrombospondin, type I, domain containing 7B	0.019	-8.168097006
1423146_at	Hes5	hairy and enhancer of split 5 (Drosophila)	0.019	-8.111675838
1454613_at	Dpysl3	dihydropyrimidinase-like 3	0.019	-8
1416410_at	Pafah1b3	platelet-activating factor acetylhydrolase, isoform 1b, subunit	0.019	-8
1448205_at	Gm5593///Ccnb1	predicted gene 5593///cyclin B1	0.019	-8
1424278_a_at	Birc5	baculoviral IAP repeat-containing 5	0.0214	-7.835362381
1438852_x_at	Mcm6	minichromosome maintenance complex component 6	0.019	-7.727490631
1450842_a_at	Cenpa	centromere protein A	0.019	-7.621103984
1422134_at	Fosb	FBJ osteosarcoma oncogene B	0.019	-7.621103984
1418334_at	Dbf4	DBF4 zinc finger	0.019	-7.568461174
1456344_at	Tnc	tenascin C	0.0274	-7.568461174
1424764_at	Sez6l	seizure related 6 homolog like	0.019	-7.516181994
1435963_at	Sema5b	sema domain, seven thrombospondin repeats (type 1 and type	0.0199	-7.516181994
1441536_at	Hmgcs1	3-hydroxy-3-methylglutaryl-Coenzyme A synthase 1	0.0267	-7.464263932
1436907_at	Nav1	neuron navigator 1	0.019	-7.412704495
1452242_at	Cep55	centrosomal protein 55	0.019	-7.361501205
1424046_at	Bub1	BUB1, mitotic checkpoint serine/threonine kinase	0.019	-7.160200567
1416266_at	Pdyn	prodynorphin	0.0263	-7.160200567
1456354_at	Chrna4	cholinergic receptor, nicotinic, alpha polypeptide 4	0.0203	-7.110741449
1435338_at	Cdk6	cyclin-dependent kinase 6	0.022	-7.06162397
1456509_at	1110032F04Rik	RIKEN cDNA 1110032F04 gene	0.019	-7.06162397
1436392_s_at	Tfap2c	transcription factor AP-2, gamma	0.019	-7.06162397
1416050_a_at	Scarb1	scavenger receptor class B, member 1	0.019	-7.012845771

1438009_at	Hist1h2ao///Hist1h2	histone cluster 1, H2ao///histone cluster 1, H2ai///histone clust	0.019	-6.964404506
1451128_s_at	Kif22	kinesin family member 22	0.019	-6.964404506
1421546_a_at	Racgap1	Rac GTPase-activating protein 1	0.019	-6.964404506
1415810_at	Uhrf1	ubiquitin-like, containing PHD and RING finger domains, 1	0.019	-6.964404506
1435627_x_at	Marcksl1	MARCKS-like 1	0.019	-6.91629785
1433935_at	AU020206	expressed sequence AU020206	0.019	-6.868523492
1429171_a_at	Ncapg	non-SMC condensin I complex, subunit G	0.019	-6.868523492
1449171_at	Ttk	Ttk protein kinase	0.0199	-6.821079134
1418666_at	Ptx3	pentraxin related gene	0.019	-6.680703355
1416505_at	Nr4a1	nuclear receptor subfamily 4, group A, member 1	0.019	-6.634556367
1455622_at	Podxl2	podocalyxin-like 2	0.0253	-6.543216468
1448194_a_at	Mir675///H19	microRNA 675///H19, imprinted maternally expressed transcri	0.019	-6.453134074
1434400_at	Tgif2	TGFB-induced factor homeobox 2	0.019	-6.453134074
1419513_a_at	Ect2	ect2 oncogene	0.019	-6.408559021
1417395_at	Klf4	Kruppel-like factor 4 (gut)	0.0211	-6.408559021
1450920_at	Ccnb2	cyclin B2	0.0227	-6.36429187
1416514_a_at	Fscn1	fascin actin-bundling protein 1	0.019	-6.36429187
1452519_a_at	Zfp36	zinc finger protein 36	0.019	-6.276672783
1448777_at	Mcm2	minichromosome maintenance complex component 2	0.019	-6.233316637
1435306_a_at	Kif11	kinesin family member 11	0.0192	-6.062866266
1434767_at	Mis18bp1	MIS18 binding protein 1	0.019	-6.062866266
1441491_at	A330068G13Rik	RIKEN cDNA A330068G13 gene	0.0274	-6.062866266
1460608_at	Cacna1b	calcium channel, voltage-dependent, N type, alpha 1B subunit	0.035	-5.979396995
1441693_at	Adamts3	a disintegrin-like and metallopeptidase (reprolysin type) with t	0.019	-5.938094283
1455899_x_at	Socs3	suppressor of cytokine signaling 3	0.019	-5.938094283
1459403_at	Ldlr	low density lipoprotein receptor	0.0222	-5.897076869
1434115_at	Cdh13	cadherin 13	0.0221	-5.856342784
1416442_at	Ier2	immediate early response 2	0.019	-5.856342784
1424118_a_at	Spc25	SPC25, NDC80 kinetochore complex component, homolog (S,	0.0191	-5.735820992
1449581_at	Emid1	EMI domain containing 1	0.0199	-5.696200782
1436718_at	Nxph1	neurexophilin 1	0.019	-5.696200782
1427256_at	Vcan	versican	0.0214	-5.617779503
1442280_at	Knstrn	kinetochore-localized astrin/SPAG5 binding	0.024	-5.578974665
1427161_at	Cenpf	centromere protein F	0.019	-5.540437872
1459627_at	Msmo1	methylsterol monoxygenase 1	0.0391	-5.540437872
1441983_at	cDNA4	UI-M-BH3-aqt-d-10-0-UI.s1 NIH_BMAP_M_S4 Mus musculus cDI	0.0246	-5.502167273
1454700_at	Lrfn4	leucine rich repeat and fibronectin type III domain containing 4	0.0199	-5.464161027
1416299_at	Shcbp1	Shc SH2-domain binding protein 1	0.0199	-5.464161027
1456158_at	Draxin	dorsal inhibitory axon guidance protein	0.0259	-5.42641731
1416028_a_at	Hn1	hematological and neurological expressed sequence 1	0.019	-5.42641731
1417822_at	D17H6S56E-5	DNA segment, Chr 17, human D6S56E 5	0.0191	-5.351710219
1455272_at	Grm5	glutamate receptor, metabotropic 5	0.0199	-5.351710219
1419156_at	Sox4	SRY (sex determining region Y)-box 4	0.0199	-5.351710219
1452092_at	Chst15	carbohydrate (N-acetylgalactosamine 4-sulfate 6-O) sulfotrans	0.0232	-5.314743256
1428105_at	Tpx2	TPX2, microtubule-associated	0.025	-5.205367422
1452534_a_at	Hmgb2	high mobility group box 2	0.0222	-5.169411323

Extended Table 1. Genes statistically enriched and down-regulated in developing astrocytes. The differentially expressed genes in mature astrocytes (P30) compared to immature astrocytes (P7) are listed along with their fold-change enrichment and the Affymetrix probe set ID (Cahoy et al., 2008). All genes are statistically different by Geo2R analysis with an adjusted P-value (Benjamini and Hochberg, 1995 FDR) threshold <5%. There are 93 and 82 immature and mature astrocyte-enriched genes, respectively, selected with a 5-fold change criteria.

GOID	TERM	CORRECTED_PVALUE	NUM_LIST_ANNOTATIONS	LIST_SIZE	TOTAL_NUM_ANNOTATIONS	POPULATION_SIZE	ANNOTATED_GENES
Upregulated genes							
GO:0030054	cell junction	0.0067	13	73	1210	24808	CDH19,LYPD6,ARHGAP2,MYLK,GJB6,CLDN11,USP53,DLC1, TMEM204,LGI1,FAM107A,ABCB1a,TEK
GO:0015629	actin cytoskeleton	0.0168	8	73	505	24808	MOBP,FLT1,FAM107A,CSRP1,MYLK,GJB6,DLC1,TEK
GO:0043209	myelin sheath	0.0056	6	73	213	24808	MOBP, MYOC, MBP, ASS1, CLDN11, CNTN1
GO:0019867	outer membrane	0.0416	5	73	197	24808	MYOC, CLMN, ASS1, MAOB, ACSL3
Downregulated genes							
GO:0000278	mitotic cell cycle	1.7935e-21	32	90	833	24808	BUB1B, CENPF, CEP55, CKS2, TOP2A, MCM6, KNSTRN, UBE2C, MCM2, MKI67, SPC25, TRIP13, DBF4, CENPA, CCNB1, PRC1, KIF22, CCNA2, KLF4, CDK1, KIF11, CCNB2, PBK, ECT2, BIRC5, SOX4, NCAPG, AURKB, CDCA8, TPX2, BUB1, RACGAP1
GO:0007049	cell cycle	2.7605e-19	39	90	1673	24808	BUB1B, CENPF, CEP55, CKS2, TOP2A, MCM6, KNSTRN, UBE2C, NR4A1, MCM2, MIS18BP1, MKI67, SPC25, TRIP13, DBF4, CENPA, CCNB1, PRC1,MCM5, ESCO2, KIF22, CCNA2, MELK, UHRF1, KLF4, CDK1, KIF11, CCNB2, PBK, ECT2, BIRC5, SOX4, NCAPG, AURKB, CDCA8, TPX2, BUB1, RACGAP1, 2810417H13Rik
GO:0007059	chromosome segregation	8.6449e-15	19	90	327	24808	BUB1B, CENPF, ESCO2, KIF22, TOP2A, KNSTRN, UBE2C, MKI67, SPC25, TRIP13, ECT2, BIRC5, CCNB1, NCAPG, AURKB, CDCA8, BUB1, RACGAP1, PRC1
GO:0051301	cell division	1.7635e-13	22	90	588	24808	BUB1B, CEP55, CKS2, CCNA2, TOP2A, KNSTRN, CDK1, KIF11, UBE2C, MIS18BP1, SPC25, CCNB2, ECT2, CENPA, BIRC5, CCNB1, AURKB, CDCA8, TPX2, BUB1, PRC1, RACGAP1
GO:0000280	nuclear division	9.5614e-13	19	90	422	24808	BUB1B, CKS2, KIF22, TOP2A, KNSTRN, KIF11, UBE2C, MKI67, TRIP13, CCNB2, BIRC5, CCNB1, NCAPG, AURKB, CDCA8, TPX2, BUB1, PRC1, RACGAP1

Abbreviations:
NUM_LIST_ANNOTATIONS: number of genes from the input list that match the annotation
LIST_SIZE: number of genes in the input list
TOTAL_NUM_ANNOTATIONS: number of genes from the mouse genome that match the annotation
POPULATION_SIZE: number of genes in the mouse genome

Extented Table 2. GO Term Finder analysis of genes upregulated and downregulated in mature vs immature astrocytes. Selected lists of differentially expressed genes (93 down- and 82 up-regulated genes) were analyzed for GO terms selecting “process” for immature associated genes and “component” for mature ones. Whereas immature astrocytes are characterized by intensive cell division, mature astrocytes present enrichment in genes involved in cell junction.

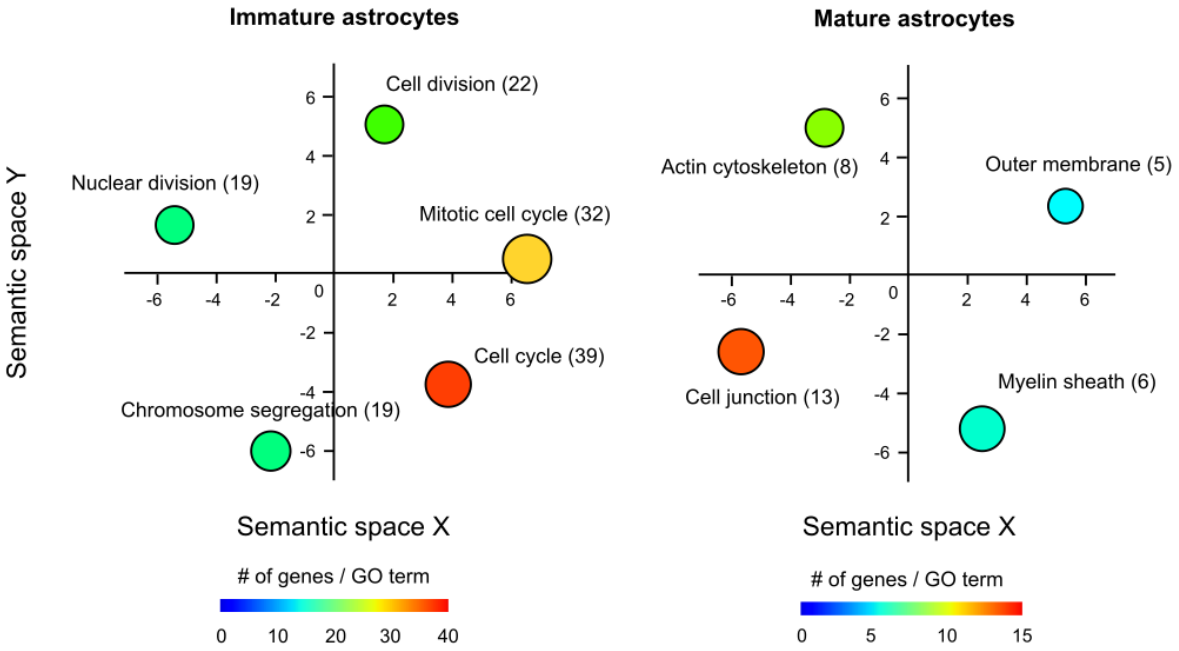

Extended Figure 1. Semantic similarity-based scatterplots of GO terms. GO terms (Extended Data Table 2) identified through the analysis of down or up-regulated genes (Extended Data Table 1) respectively associated to immature (P7) and mature (P30) astrocytes and visualized according to the similarity of the GO terms along arbitrary X and Y axis. Each circle is color-coded according to the frequency of the GO term in the EBI GOA reference database, and the number of genes per GO term is indicated in parenthesis. Circle size indicates the P-value (circles with bigger size have smaller P value) (Extended Table 2).

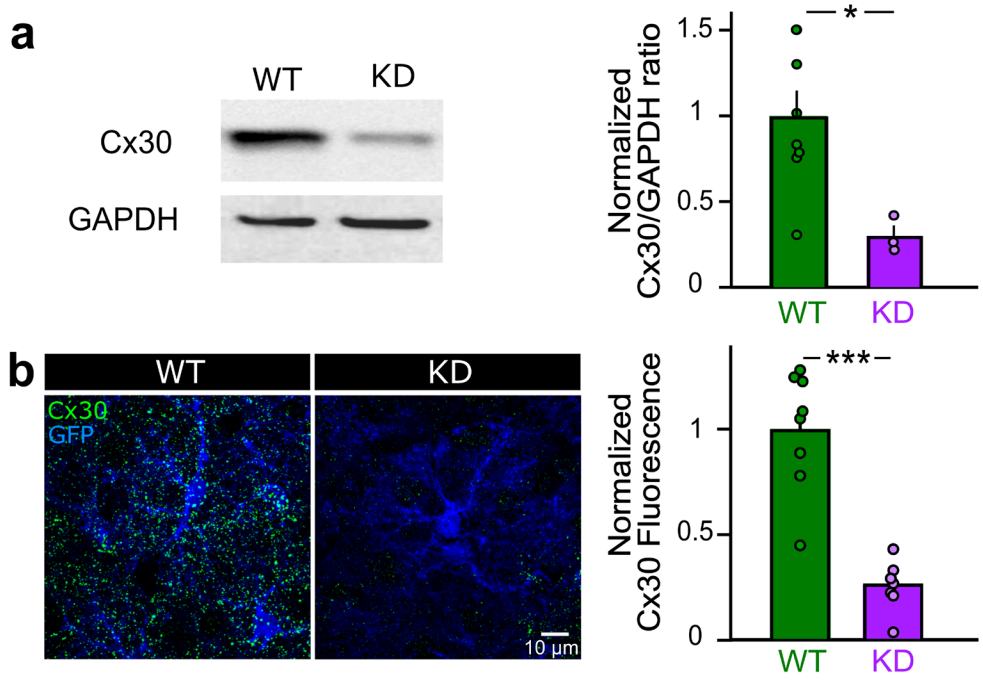

Extended Figure 2. Characterization of Cx30 KD mice. (a) Western blot analysis from visual cortex shows a decrease of 70% in Cx30 expression in KD mice (n=3) compared to WT mice (n=8, P=0.0242, U=1, Mann-Whitney test). (b) Immunostaining of Cx30 in the visual cortex also shows a 70% decrease in Cx30 expression in astrocytes in KD mice (n=7 samples from 3 mice) compared to WT mice (n=8 samples from 3 mice, P=0.0003, U=0, Mann-Whitney test).

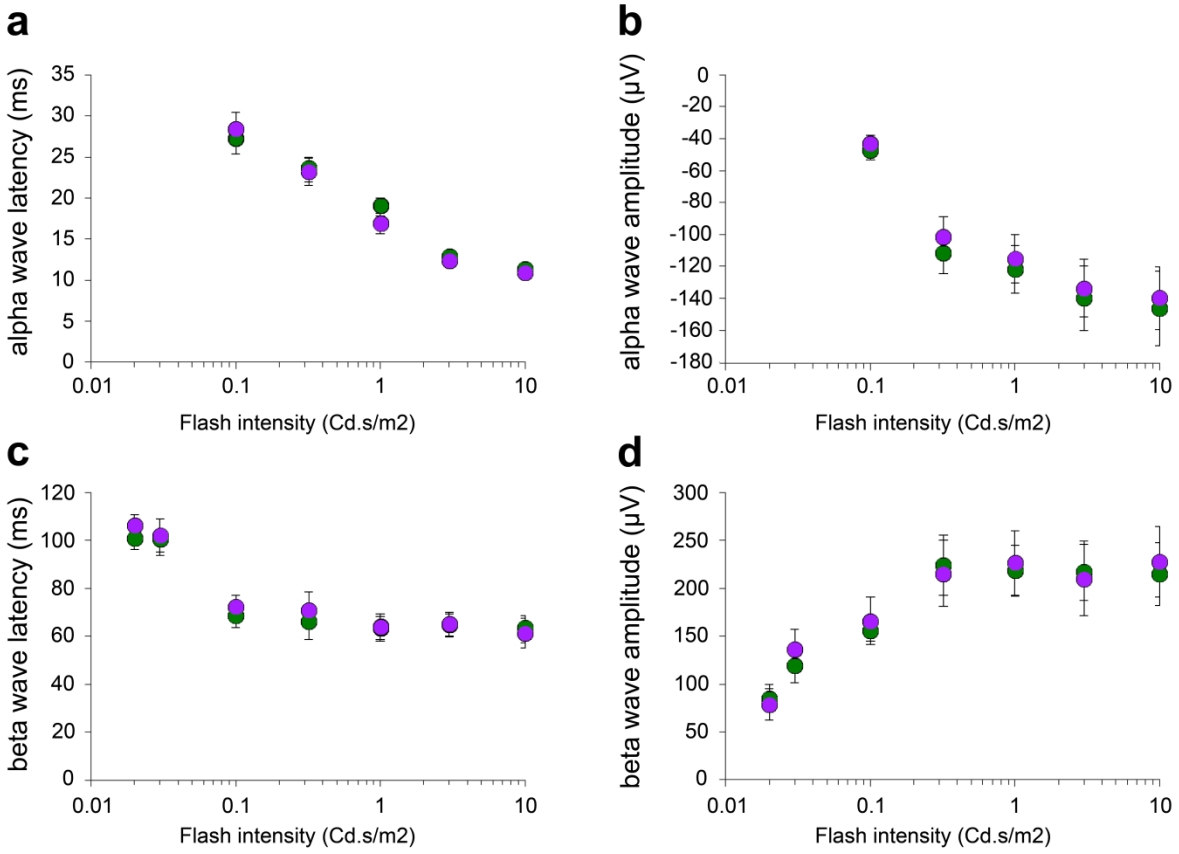

Extended Figure 3. Retinal activation is unchanged in KD mice. The changes in potentials induced by light flashes of increasing intensity (from 0.02 to 10 Cd.s/m2) in the retinal tissue was assessed by recording alpha- and beta-wave latency and amplitude. No difference in electroretinograms were detected between WT (n=6) and KD mice (n=6, alpha wave latency: P=0.5550, DF=50, F(1,50)=0.3531; alpha wave amplitude: P=0.6231, DF=50, F(1,50)=0.2446; beta wave latency: P=0.5278, DF=71, F(1,71)=0.4027; beta wave amplitude: P=0.8016, DF=70, F(1,70)=0.06365; 2-way ANOVA).

146/2164	Gene & Synonyms	WFA WT /KD						Total	MW	Description	Species
		Ratio	Log2	Adj. p-value	CV %	Distinct peptide used	Peptide used				
P61759	Vbp1,Pfdn3	1000.00	1000.00			1	4	4	22.4	Prefoldin subunit 3	Mus musculus
Q8CES0	Naa30,Mak3,Nat12	1000.00	1000.00			1	3	3	39.4	N-alpha-acetyltransferase 30	Mus musculus
Q9EQG3	Scel	809.52	9.66			1	4	4	73.0	Sciellin	Mus musculus
O35551	Rabep1,Rab5ep,Rabpt5,Rabpt5a	134.15	7.07			1	3	3	99.5	Rab GTPase-binding effector protein 1	Mus musculus
O54988	Slk,Kiaa0204,Stk2	3.20	1.68	2.39E-06	15.59530284	11	67	69	141.5	STE20-like serine/threonine-protein kinase	Mus musculus
Q8QZX0	Sbk1,Sbk	2.90	1.54	0.006079	0.075393677	1	5	5	45.7	Serine/threonine-protein kinase SBK1	Mus musculus
Q8CJ19	Mical3,Kiaa0819,Kiaa1364	2.85	1.51	0.004016	21.25373328	5	26	30	223.7	[F-actin]-monooxygenase MICAL3	Mus musculus
P68404	Prkcb,Pkcb,Prkcb1	2.66	1.41	0.002285	17.64812435	4	18	19	76.8	Protein kinase C beta type	Mus musculus
P26516	Psmd7,Mov-34,Mov34	2.56	1.36	2.9E-05	13.76946143	4	27	31	36.5	26S proteasome non-ATPase regulatory subunit 7	Mus musculus
Q8K3I9	Glcci1,Gig18,Tssn1	2.51	1.33	0.026854	19.02016517	2	11	17	57.5	Glucocorticoid-induced transcript 1 protein	Mus musculus
P54254	Atxn1,Sca1	2.48	1.31	2.27E-05	14.31049909	6	30	32	83.8	Ataxin-1	Mus musculus
Q76LL6	Fhod3,Fhos2,Kiaa1695	2.32	1.21	0.013662	12.80855473	2	9	11	175.7	FH1/FH2 domain-containing protein 3	Mus musculus
O88738	Birc6,Kiaa1289	2.25	1.17	0.010948	20.16502341	3	14	15	532.2	Baculoviral IAP repeat-containing protein 6	Mus musculus
Q62446	Fkbp3,Fkbp25	2.20	1.14	0.00019	20.34046107	10	75	76	25.1	Peptidyl-prolyl cis-trans isomerase FKBP3	Mus musculus
P52480	Pkm,Pk3,Pkm2,Pykm	2.17	1.12	2.81E-11	9.468352062	7	55	57	57.8	Pyruvate kinase PKM	Mus musculus
Q80XI3	Eif4g3	2.16	1.11	1.09E-15	7.882255709	10	77	88	174.9	Eukaryotic translation initiation factor 4 gamma 3	Mus musculus
A2AN08	Ubr4,Kiaa0462,Zubr1	2.13	1.09	0.001063	20.53598837	7	36	39	572.3	E3 ubiquitin-protein ligase UBR4	Mus musculus
Q3USJ8	Fchsd2,Kiaa0769,Sh3md3	2.10	1.07	0.000678	19.11699652	4	30	30	84.3	F-BAR and double SH3 domains protein 2	Mus musculus
P48678	Lmna,Lmn1	2.09	1.06	0.013662	23.00733647	3	17	21	74.2	Prelamin-A/C	Mus musculus
Q811P8	Arhgap32,Grit,Kiaa0712,Rics	2.05	1.03	7.19E-12	9.132445507	10	60	71	229.7	Rho GTPase-activating protein 32	Mus musculus
Q3THK3	Gtf2f1	2.00	1.00	0.007011	18.28659847	3	14	18	57.2	General transcription factor IIF subunit 1	Mus musculus
E9Q557	Dsp	1.99	0.99	0.00028	21.04795421	12	79	79	332.9	Desmoplakin	Mus musculus
Q8JZQ9	Eif3b,Eif3s9	1.98	0.99	0.01836	20.99918586	1	12	12	91.4	Eukaryotic translation initiation factor 3 subunit B	Mus musculus
O55143	Atp2a2	1.98	0.98	0.008788	25.3912108	5	29	34	114.9	Sarcoplasmic/endoplasmic reticulum calcium ATPase 2	Mus musculus
Q62318	Trim28,Krip1,Tif1b	1.96	0.97	7.79E-08	13.18544934	8	62	64	88.8	Transcription intermediary factor 1-beta	Mus musculus
Q3UH66	Wnk2,Kiaa1760	1.96	0.97	0.003006	20.4282488	4	22	23	227.5	Serine/threonine-protein kinase WNK2	Mus musculus
O08586	Pten,Mmac1	1.92	0.94	0.042364	27.63248399	2	15	16	47.2	Phosphatidylinositol 3,4,5-trisphosphate 3-phosphatase and dual-specificity protein phosphatase PTEN	Mus musculus
O35385	Ppef2	1.91	0.94	0.001789	12.79143067	1	12	12	86.6	Serine/threonine-protein phosphatase with EF-hands 2	Mus musculus
Q6DFZ1	Gbf1	1.91	0.94	5.33E-09	10.07331619	6	42	42	206.8	Golgi-specific brefeldin A-resistance factor 1	Mus musculus
Q9QYR6	Map1a,Mtap1,Mtap1a	1.91	0.93	1.08E-08	14.76681154	53	290	302	300.1	Microtubule-associated protein 1A	Mus musculus
O88447	**Klc1,Kns2**	**1.91**	**0.93**	**6.56E-11**	**7.79711168**	**8**	**39**	**52**	**61.5**	**Kinesin light chain 1**	**Mus musculus**
P33175	**Kif5a,Kiaa4086,Kif5,Nkhc1**	**1.89**	**0.92**	**0.048086**	**26.18822758**	**2**	**12**	**12**	**117.0**	**Kinesin heavy chain isoform 5A**	**Mus musculus**
Q9DBS5	**Klc4,Knsl8**	**1.89**	**0.92**	**0.007071**	**18.34439877**	**2**	**14**	**17**	**68.6**	**Kinesin light chain 4**	**Mus musculus**
Q8CDA1	Inpp5f,Kiaa0966,Sac2	1.84	0.88	2.29E-08	11.95669286	8	55	66	127.6	Phosphatidylinositide phosphatase SAC2	Mus musculus
P33173	Kif1a,Atsv,Kif1	1.83	0.87	1.65E-05	14.82556407	5	35	40	191.7	Kinesin-like protein KIF1A	Mus musculus
Q3UYC0	Ppm1h,Kiaa1157	1.80	0.85	2.11E-05	15.26105258	4	37	47	56.4	Protein phosphatase 1H	Mus musculus
Q80ZJ7	Snx32,Snx6b	1.79	0.84	0.003708	12.99945429	2	11	12	46.6	Sorting nexin-32	Mus musculus
O35382	Exoc4,Sec8,Sec8l1	1.79	0.84	0.032487	20.04872335	1	10	12	110.5	Exocyst complex component 4	Mus musculus
Q61768	**Kif5b,Khcs,Kns1**	**1.75**	**0.81**	**2.2E-06**	**14.63427064**	**8**	**50**	**54**	**109.6**	**Kinesin-1 heavy chain**	**Mus musculus**
P42859	Htt,Hd,Hdh	1.74	0.80	0.010867	25.76552188	5	27	29	344.7	Huntingtin	Mus musculus
P54822	Adsl,Adl	1.74	0.80	0.024474	23.71478869	2	14	18	54.9	Adenylosuccinate lyase	Mus musculus
Q61879	Myh10	1.74	0.80	6.48E-27	5.896485627	20	122	146	229.0	Myosin-10	Mus musculus
Q6PD10	Ip6k1,Ihpk1	1.73	0.79	0.049286	14.9523868	2	8	8	49.3	Inositol hexakisphosphate kinase 1	Mus musculus
Q91WG7	Dgkg,Dagk3	1.73	0.79	0.020893	26.6598409	4	20	23	88.5	Diacylglycerol kinase gamma	Mus musculus
Q3USB7	Plcl1	1.73	0.79	0.004272	24.04496638	7	36	38	122.7	Inactive phospholipase C-like protein 1	Mus musculus
P52623	Uck1,Umpk	1.71	0.77	0.000174	16.60444341	3	28	28	31.1	Uridine-cytidine kinase 1	Mus musculus
Q8CI94	Pygb	1.70	0.77	0.01997	28.16517117	5	26	29	96.7	Glycogen phosphorylase, brain form	Mus musculus
F6SEU4	Syngap1	1.68	0.75	0.008479	26.43766935	5	38	40	148.2	Ras/Rap GTPase-activating protein SynGAP	Mus musculus
Q8BMF4	Dlat	1.67	0.74	1.67E-05	13.97343485	6	31	36	67.9	Dihydrolipoyllysine-residue acetyltransferase component of pyruvate dehydrogenase complex, mitochondrial	Mus musculus
Q6P1I6	Psd2	1.67	0.74	0.015629	24.89529792	3	18	18	84.3	PH and SEC7 domain-containing protein 2	Mus musculus
Q9DB27	Mcts1	1.67	0.74	0.009234	23.78461434	3	21	23	20.6	Malignant T-cell-amplified sequence 1	Mus musculus
Q7TQF7	Amph,Amph1	1.67	0.74	1.87E-14	8.819239129	13	86	102	75.0	Amphiphysin	Mus musculus
Q8CGC7	Eprs,Qprs	1.66	0.73	3.49E-12	11.6193788	24	166	174	170.1	Bifunctional glutamate/proline--tRNA ligase	Mus musculus
P70290	Mpp1	1.64	0.71	0.000675	18.54377691	4	28	30	52.2	55 kDa erythrocyte membrane protein	Mus musculus
Q9D8U8	Snx5	1.63	0.71	1.34E-06	12.46985036	6	34	36	46.8	Sorting nexin-5	Mus musculus
P28738	Kif5c,Nkhc2	1.63	0.70	6.6E-06	16.75823116	11	77	90	109.3	Kinesin heavy chain isoform 5C	Mus musculus
Q80XQ2	Tbc1d5	1.63	0.70	0.003155	21.57073782	5	26	27	91.8	TBC1 domain family member 5	Mus musculus
Q8VDN4	Ccdc92,D5Bwg0834e	1.61	0.69	0.000675	21.33832429	6	52	57	35.2	Coiled-coil domain-containing protein 92	Mus musculus
O08919	Numbl,Nbl	1.59	0.67	0.004506	23.54602998	2	30	30	64.1	Numb-like protein	Mus musculus
Q9DBC3	Cmtr1,Ftsjd2,Kiaa0082	1.57	0.65	0.007106	20.36903894	2	16	18	95.7	Cap-specific mRNA (nucleoside-2'-O-)-methyltransferase 1	Mus musculus
Q6NZL0	Soga3	1.57	0.65	0.008788	26.07925649	5	34	37	103.5	Protein SOGA3	Mus musculus
Q9CQ79	Txndc9,Apacd	1.56	0.64	0.004261	24.15682851	5	37	37	26.3	Thioredoxin domain-containing protein 9	Mus musculus
Q62420	Sh3gl2,Sh3d2a	1.56	0.64	3.38E-06	14.26796973	5	43	49	40.0	Endophilin-A1	Mus musculus
Q8BG92	Clvs2,Rlbp1l2	1.55	0.64	0.010697	23.3728237	2	18	18	38.0	Clavesin-2	Mus musculus
Q8VHJ5	Mark1,Emk3,Kiaa1477	1.55	0.64	0.023248	30.31749528	4	37	40	88.3	Serine/threonine-protein kinase MARK1	Mus musculus
Q8CHC4	Synj1,Kiaa0910	1.55	0.63	4.84E-12	12.10563611	31	224	230	172.6	Synaptojanin-1	Mus musculus
Q8K394	Plcl2,Kiaa1092,Plce2	1.53	0.62	3.03E-05	16.47086309	7	44	58	125.8	Inactive phospholipase C-like protein 2	Mus musculus
D3YZU1	Shank1	1.52	0.61	0.001217	21.54012545	8	41	44	226.3	SH3 and multiple ankyrin repeat domains protein 1	Mus musculus
Q9ES97	Rtn3	1.52	0.60	0.004016	24.84622418	10	52	67	103.9	Reticulon-3	Mus musculus
P51174	Acadl	0.66	-0.59	6.6E-06	12.10153131	5	27	34	47.9	Long-chain specific acyl-CoA dehydrogenase, mitochondrial	Mus musculus
Q8BGQ7	Aars	0.66	-0.59	0.005213	26.15965795	10	61	69	106.9	Alanine--tRNA ligase, cytoplasmic	Mus musculus
P38647	Hspa9,Grp75,Hsp74,Hspa9a	0.66	-0.60	0.000686	21.28143564	8	50	56	73.5	Stress-70 protein, mitochondrial	Mus musculus
Q922Q4	Pycr2	0.66	-0.60	0.024273	18.44134176	2	10	11	33.7	Pyrroline-5-carboxylate reductase 2	Mus musculus
Q62165	Dag1,Dag-1	0.65	-0.61	0.002788	18.75329902	2	18	18	96.9	Dystroglycan	Mus musculus
Q62188	Dpysl3,Drp3,Ulip	0.65	-0.62	1.04E-06	13.51874369	5	44	47	61.9	Dihydropyrimidinase-related protein 3	Mus musculus
Q920P5	Ak5	0.65	-0.62	0.033937	32.88881184	8	49	56	63.3	Adenylate kinase isoenzyme 5	Mus musculus
Q7TN29	Smap2,Smap11	0.65	-0.63	2.7E-05	15.37998954	4	34	35	46.6	Stromal membrane-associated protein 2	Mus musculus
Q9DCW4	Etfb	0.64	-0.64	0.002068	23.40384061	6	48	48	27.6	Electron transfer flavoprotein subunit beta	Mus musculus
Q9JKY5	Hip1r	0.64	-0.64	0.000462	20.73315839	10	55	69	119.4	Huntingtin-interacting protein 1-related protein	Mus musculus
P21981	Tgm2	0.64	-0.65	0.01069	21.10408291	2	15	17	77.1	Protein-glutamine gamma-glutamyltransferase 2	Mus musculus
Q91VJ5	Pqbp1,Npw38	0.64	-0.65	0.026627	5.719685746	1	6	6	30.6	Polyglutamine-binding protein 1	Mus musculus
Q8R001	Mapre2	0.63	-0.66	0.012228	28.64501901	10	51	60	36.9	Microtubule-associated protein RP/EB family member 2	Mus musculus
O08585	Clta	0.63	-0.67	2.68E-06	10.88919057	2	24	24	25.6	Clathrin light chain A	Mus musculus
Q9Z1P6	Ndufa7	0.63	-0.67	0.003205	19.11087114	3	19	24	12.6	NADH dehydrogenase [ubiquinone] 1 alpha subcomplex subunit 7	Mus musculus
Q8K3H0	Appl1,Dip13a,Kiaa1428	0.62	-0.68	0.003607	17.06072203	2	15	18	79.3	DCC-interacting protein 13-alpha	Mus musculus
Q71LX4	Tln2	0.62	-0.68	0.000163	21.35196305	31	189	191	253.6	Talin-2	Mus musculus
P97315	Csrp1,Crp1,Csrp	0.62	-0.68	1.14E-05	16.27098768	7	53	58	20.6	Cysteine and glycine-rich protein 1	Mus musculus
Q3UHJ0	Aak1,Kiaa1048	0.62	-0.69	4.13E-09	13.12857526	17	108	130	103.3	AP2-associated protein kinase 1	Mus musculus
P99029	Prdx5,Prdx6	0.62	-0.70	2.68E-08	11.44280753	7	45	46	21.9	Peroxiredoxin-5, mitochondrial	Mus musculus
Q810A7	Ddx42	0.61	-0.70	0.000423	20.28254695	8	47	50	102.0	ATP-dependent RNA helicase DDX42	Mus musculus
Q03265	Atp5a1	0.61	-0.71	4.64E-07	13.87154214	9	58	73	59.8	ATP synthase subunit alpha, mitochondrial	Mus musculus
Q9D0E3	Lysmd1	0.61	-0.72	0.01534	23.47202056	3	16	18	24.8	LysM and putative peptidoglycan-binding domain-containing protein 1	Mus musculus
Q6PB44	Ptpn23,Kiaa1471	0.61	-0.72	0.001859	20.34852808	5	26	26	185.2	Tyrosine-protein phosphatase non-receptor type 23	Mus musculus
Q3UHD9	Agap2,Centg1,Kiaa0167	0.60	-0.74	2.64E-05	17.63216822	8	63	69	124.5	Arf-GAP with GTPase, ANK repeat and PH domain-containing protein 2	Mus musculus
Q99K01	Pdxdc1	0.60	-0.74	0.001835	22.46675189	7	41	44	87.3	Pyridoxal-dependent decarboxylase domain-containing protein 1	Mus musculus
P26039	Tln1,Tln	0.60	-0.74	5.59E-05	19.41068781	17	98	105	269.8	Talin-1	Mus musculus
P08553	Nefm,Nef3,Nfm	0.60	-0.74	0.000894	15.4988097	2	17	18	95.9	Neurofilament medium polypeptide	Mus musculus
P59759	Mkl2,Mrtfb	0.60	-0.74	0.000361	18.00130202	5	30	34	117.5	Myocardin-related transcription factor B	Mus musculus
Q7SIG6	Asap2,Ddef2,Gm1523,Gm592	0.60	-0.75	0.01693	26.56912474	4	23	27	106.8	Arf-GAP with SH3 domain, ANK repeat and PH domain-containing protein 2	Mus musculus
O08749	Dld	0.59	-0.75	0.001133	22.82803651	9	64	66	54.3	Dihydrolipoyl dehydrogenase, mitochondrial	Mus musculus
P46660	Ina	0.59	-0.76	0.047122	26.0321697	3	13	17	55.4	Alpha-internexin	Mus musculus
O88492	Plin4,Kiaa1881	0.59	-0.77	0.007061	22.24949292	4	20	23	139.4	Perilipin-4	Mus musculus
Q80X50	Ubap2l	0.58	-0.79	0.005682	25.77866756	10	49	52	116.8	Ubiquitin-associated protein 2-like	Mus musculus
Q91ZA3	Pcca	0.58	-0.79	7.84E-13	8.66981497	8	63	81	79.9	Propionyl-CoA carboxylase alpha chain, mitochondrial	Mus musculus
Q61548	Snap91	0.57	-0.80	0.009377	27.94765994	9	55	63	91.9	Clathrin coat assembly protein AP180	Mus musculus
Q9DCX2	Atp5h	0.57	-0.81	0.027797	29.47730013	3	24	24	18.7	ATP synthase subunit d, mitochondrial	Mus musculus
P26443	Glud1,Glud	0.57	-0.82	1.22E-05	15.57543874	6	45	53	61.3	Glutamate dehydrogenase 1, mitochondrial	Mus musculus

Q9DB20	Atp5o,D12Wsu28e	0.56	-0.83	7.24E-05	13.71695369	3	22	24	23.4	ATP synthase subunit O, mitochondrial	Mus musculus
Q8CCT4	Tceal5	0.55	-0.85	0.006079	14.63484766	3	12	13	22.0	Transcription elongation factor A protein-like 5	Mus musculus
P35700	Prdx1,Msp23,Paga,Tdpx2	0.55	-0.85	0.025661	27.11931534	3	18	18	22.2	Peroxiredoxin-1	Mus musculus
P41242	Matk,Ctk,Ntk	0.55	-0.86	0.035669	20.56916551	2	10	11	56.1	Megakaryocyte-associated tyrosine-protein kinase	Mus musculus
A0A0N4SVR5	Rasgef1a	0.55	-0.87	0.045892	7.871596314	1	6	6	56.9	RasGEF domain family, member 1A	Mus musculus
Q9D8S3	Arfgap3	0.54	-0.88	1.61E-06	11.71431444	6	30	36	57.5	ADP-ribosylation factor GTPase-activating protein 3	Mus musculus
Q9JJC6	Rilpl1,MNCb-2440	0.54	-0.90	0.028843	29.9009786	5	28	37	47.3	RILP-like protein 1	Mus musculus
Q9CQ48	Nudcd2,D11Ertd603e	0.54	-0.90	0.028872	12.02288632	2	8	11	17.7	NudC domain-containing protein 2	Mus musculus
Q7TNC4	Luc7l2	0.54	-0.90	2.49E-09	10.91811889	7	53	56	46.6	Putative RNA-binding protein Luc7-like 2	Mus musculus
Q8K2K6	Agfg1,Hrb,Rip	0.53	-0.91	0.006597	25.50988852	5	36	36	58.0	Arf-GAP domain and FG repeat-containing protein 1	Mus musculus
Q6P542	Abcf1	0.52	-0.93	3.57E-06	11.54959357	4	26	29	94.9	ATP-binding cassette sub-family F member 1	Mus musculus
Q9D1P4	Chordc1,Chp1,Morgana	0.51	-0.96	0.008763	26.5546428	6	39	43	37.4	Cysteine and histidine-rich domain-containing protein 1	Mus musculus
Q9JMD0	Znf207,Bugz,Zep,Zfp207	0.51	-0.98	0.008255	23.99580676	3	23	24	52.8	BUB3-interacting and GLEBS motif-containing protein ZNF207	Mus musculus
Q3UTH8	Arhgef9,Kiaa0424	0.50	-1.01	0.006597	12.78098887	1	10	10	60.9	Rho guanine nucleotide exchange factor 9	Mus musculus
P17751	Tpi1,Tpi	0.50	-1.01	1.99E-13	7.317211555	5	47	48	32.2	Triosephosphate isomerase	Mus musculus
Q569Z5	Ddx46,Kiaa0801	0.49	-1.02	2.69E-06	14.33116647	6	44	44	117.4	Probable ATP-dependent RNA helicase DDX46	Mus musculus
Q9QZQ1	Mllt4,Af6	0.49	-1.03	8.97E-06	12.42007126	5	26	27	206.5	Afadin	Mus musculus
E9Q6E5	Srsf11 {ECO:0000313|Ensembl:EN	0.49	-1.04	0.000405	17.0504658	3	24	24	56.7	Serine/arginine-rich-splicing factor 11	Mus musculus
Q8K4G5	Ablim1,Ablim,Kiaa0059	0.48	-1.06	3.81E-08	10.59657982	5	36	36	96.8	Actin-binding LIM protein 1	Mus musculus
Q8CEC5	Nkiras1	0.48	-1.07	0.008788	21.9007149	3	17	17	21.7	NF-kappa-B inhibitor-interacting Ras-like protein 1	Mus musculus
Q6NVF9	Cpsf6	0.47	-1.09	2.2E-06	13.08770585	5	35	35	59.2	Cleavage and polyadenylation specificity factor subunit 6	Mus musculus
E9PV24	Fga {ECO:0000313|Ensembl:ENSM	0.46	-1.11	3.13E-07	9.939615358	4	27	28	87.4	Fibrinogen alpha chain	Mus musculus
Q3UEB3	Puf60	0.45	-1.16	0.0092	18.06794244	3	13	16	60.2	Poly(U)-binding-splicing factor PUF60	Mus musculus
Q62418	Dbnl,Abp1,Sh3p7	0.45	-1.16	0.000339	15.50077896	4	22	26	48.7	Drebrin-like protein	Mus musculus
Q9QYH6	Maged1,Nrage	0.44	-1.19	0.008788	21.8912355	3	17	17	85.7	Melanoma-associated antigen D1	Mus musculus
Q9R0P9	Uchl1	0.40	-1.34	4.32E-08	9.046090987	4	28	30	24.8	Ubiquitin carboxyl-terminal hydrolase isozyme L1	Mus musculus
G3XA57	Rab11fip2	0.38	-1.38	0.000153	13.07310491	3	19	20	58.2	Rab11 family-interacting protein 2	Mus musculus
Q80TZ3	Dnajc6,Kiaa0473	0.36	-1.47	0.000209	15.19830231	3	23	27	102.3	Putative tyrosine-protein phosphatase auxilin	Mus musculus
Q6ZQ82	Arhgap26,Kiaa0621	0.34	-1.57	0.006097	12.48430392	2	10	11	92.1	Rho GTPase-activating protein 26	Mus musculus
Q9CW79	Golga1	0.33	-1.59	0.000147	13.00066363	5	20	22	87.3	Golgin subfamily A member 1	Mus musculus
Q8BG95	**Ppp1r12b,Mypt2**	**0.33**	**-1.59**	**0.018806**	**19.44097598**	**1**	**11**	**11**	**109.0**	**Protein phosphatase 1 regulatory subunit 12B**	**Mus musculus**
Q99MR8	Mccc1,Mcca	0.29	-1.77	9.64E-06	12.14224409	3	24	24	79.3	Methylcrotonoyl-CoA carboxylase subunit alpha, mitochondrial	Mus musculus
Q80WC7	Agfg2,Hrbl,Rabr	0.29	-1.78	0.012824	12.56489419	2	9	12	49.0	Arf-GAP domain and FG repeat-containing protein 2	Mus musculus
Q68FD9	Kiaa1549	0.27	-1.89	0.01069	14.76231614	2	10	10	209.2	UPF0606 protein KIAA1549	Mus musculus
Q9DBR7	**Ppp1r12a,Mypt1**	**0.22**	**-2.17**	**1.45E-05**	**15.04051788**	**6**	**38**	**38**	**115.0**	**Protein phosphatase 1 regulatory subunit 12A**	**Mus musculus**
B1AR51	Dnah9,Dnahc9,RP23-215H18.2-001	0.00	-1000.00			1	3	3	512.4	Dynein, axonemal, heavy chain 9	Mus musculus
P47738	Aldh2,Ahd-1,Ahd1	0.00	-1000.00			1	3	3	56.5	Aldehyde dehydrogenase, mitochondrial	Mus musculus
Q8CGY8	Ogt	0.00	-1000.00			1	3	3	117.0	UDP-N-acetylglucosamine--peptide N-acetylglucosaminyltransferase 110 kDa subunit	Mus musculus
Q91WV0	Dr1	0.00	-1000.00			1	3	3	19.4	Protein Dr1	Mus musculus

Extented Table 3. List of the WFA protein partners. Analysis of the changing WFA interactors in WT vs KD mice. In WT cells, 70 proteins were enriched or unique (log2 ratio=1000) compared to Cx30 KD cells (with the following parameters: number of peptides≥3, ratio≥1.5 and p-value≤0.05), while in Cx30 KD cells 77 proteins were enriched or unique (log2 ratio = -1000) compared to WT cells (with the following parameters: number of peptides≥3, ratio≥1/1.5 and p-value≤0.05). WT and KD proteins are highlighted in red and green, respectively. Protein from the pathways Rho GTPase activate KTN1 (bold green) and Rho GTPase activate ROCK (bold red) are indicated.

361/2370 proteins	Gene & Synonyms	Cx30 WT/KD						Total	MW	Description	Species
		Ratio	Log2	Adj. p-value	CV %	Distinct peptide used	Peptide used				
P04919	Slc4a1,Ae1	1000.00	1000.00			1	5	5	103.1	Band 3 anion transport protein	Mus musculus
Q9QXQ1	Pde7b	1000.00	1000.00			1	5	5	51.3	cAMP-specific 3',5'-cyclic phosphodiesterase 7B	Mus musculus
Q9R087	Gpc6	1000.00	1000.00			1	5	5	63.1	Glypican-6	Mus musculus
P11031	Sub1,Pc4,Rpo2tc1	1000.00	1000.00			1	4	4	14.4	Activated RNA polymerase II transcriptional coactivator p15	Mus musculus
Q8BQU6	Gjc2,Gja12	1000.00	1000.00			1	3	3	47.0	Gap junction gamma-2 protein	Mus musculus
Q8C0L8	Cog5	1000.00	1000.00			1	3	3	91.4	Conserved oligomeric Golgi complex subunit 5	Mus musculus
Q8VC31	Ccdc9	1000.00	1000.00			1	3	3	61.4	Coiled-coil domain-containing protein 9	Mus musculus
Q9JMG3	Tmub1,Hops	1000.00	1000.00			1	3	3	26.3	Transmembrane and ubiquitin-like domain-containing protein 1	Mus musculus
Q8R3I2	Mboat2,Lpcat4,Oact2	5.53	2.47	0.0029	15.27824861	1	8	8	59.0	Lysophospholipid acyltransferase 2	Mus musculus
A0A1D5RLM8	Gm11639	3.79	1.92	0.0265	26.08713593	1	8	9	654.2	Predicted gene 11639	Mus musculus
Q3U0L2	Ankrd33b	3.25	1.70	0.0294	26.84235247	1	8	8	53.2	Ankyrin repeat domain-containing protein 33B	Mus musculus
P0C673	Igsf11	3.20	1.68	0.0248	25.65673496	1	8	8	46.1	Immunoglobulin superfamily member 11	Mus musculus
Q4U2R1	Herc2,Jdf2,Kiaa0393,Rjs	3.02	1.59	0.0175	23.28784987	1	8	8	527.5	E3 ubiquitin-protein ligase HERC2	Mus musculus
Q05D44	Eif5b,If2	2.79	1.48	0.0139	16.63238791	1	6	6	137.6	Eukaryotic translation initiation factor 5B	Mus musculus
P23242	Gja1,Cxn-43	2.74	1.46	4E-35	5.270050708	16	135	142	43.0	Gap junction alpha-1 protein	Mus musculus
O09012	Pex5,Pxr1	2.53	1.34	0.03	26.96009055	1	8	8	70.8	Peroxisomal targeting signal 1 receptor	Mus musculus
Q80U35	Arhgef17,Kiaa0337	2.48	1.31	0.001	10.03391809	1	7	8	221.7	Rho guanine nucleotide exchange factor 17	Mus musculus
Q9Z0U0	Xpr1,Syg1	2.43	1.28	0.0012	17.76751762	2	13	15	81.8	RecName: Full=Xenotropic and polytropic retrovirus receptor 1; AltName: Full=Protein SYG1 homolog; AltName: Full=Rmc-1	Mus musculus
P58390	Kcnn2,Sk2	2.36	1.24	0.0242	23.26853301	1	7	8	91.6	Small conductance calcium-activated potassium channel protein 2	Mus musculus
Q78IK4	Apool,Fam121a,Mic27	2.25	1.17	0.0028	21.65556978	2	15	15	29.3	MICOS complex subunit Mic27	Mus musculus
Q9JKC6	Cend1,Bm88	2.15	1.11	6E-06	18.2372205	7	84	109	15.0	Cell cycle exit and neuronal differentiation protein 1	Mus musculus
Q8VHG2	Amot,Kiaa1071	2.15	1.11	2E-06	10.62478604	3	18	21	120.9	Angiomotin	Mus musculus
Q08460	Kcnma1,Kcnma	2.08	1.06	0.0208	33.26709837	2	28	32	134.4	Calcium-activated potassium channel subunit alpha-1	Mus musculus
Q920M5	Coro6	2.05	1.04	0.0488	30.92361688	1	8	8	52.6	Coronin-6	Mus musculus
Q99M74	Krt82,Krt2-20,Krthb2	2.05	1.03	0.0196	21.73252443	1	7	8	57.1	Keratin, type II cuticular Hb2	Mus musculus
Q9WTR1	Trpv2,Grc	2.05	1.03	0.0002	16.87816127	2	19	24	86.0	Transient receptor potential cation channel subfamily V member 2	Mus musculus
Q9Z0J4	Nos1	2.01	1.01	1E-14	10.71536481	15	147	152	160.5	Nitric oxide synthase, brain	Mus musculus
Q9CQR2	Rps21	2.01	1.01	0.0011	19.57758473	2	16	16	9.1	40S ribosomal protein S21	Mus musculus
P03995	Gfap	1.99	1.00	2E-11	11.75390763	11	89	92	49.9	Glial fibrillary acidic protein	Mus musculus
Q8C0C4	Ccser1,Fam190a,Kiaa1680	1.96	0.97	0.0495	34.70524014	2	12	14	98.2	Serine-rich coiled-coil domain-containing protein 1	Mus musculus
Q3UEB3	Puf60	1.95	0.97	0.0086	25.21148427	2	14	16	60.2	Poly(U)-binding-splicing factor PUF60	Mus musculus
Q6PHZ2	Camk2d,Kiaa4163	1.95	0.96	0.0095	27.50533056	3	19	23	56.4	Calcium/calmodulin-dependent protein kinase type II subunit delta	Mus musculus
Q8CGY8	Ogt	1.93	0.95	0.0042	14.30719524	1	7	8	117.0	UDP-N-acetylglucosamine--peptide N-acetylglucosaminyltransferase 110 kDa subunit	Mus musculus
P83870	Phf5a	1.93	0.95	0.0209	19.07489568	1	6	7	12.4	PHD finger-like domain-containing protein 5A	Mus musculus
Q8BQ30	Ppp1r18	1.93	0.95	0.0099	14.95732224	1	6	7	65.6	Phostensin	Mus musculus
Q80YS6	Afap1,Kiaa3018	1.92	0.94	0.0013	20.01038991	2	16	17	80.6	Actin filament-associated protein 1	Mus musculus
Q80SY4	Mib1,Dip1,Kiaa1323,Mib	1.92	0.94	0.0106	26.72801362	2	15	16	110.1	E3 ubiquitin-protein ligase MIB1	Mus musculus
P43006	Slc1a2,Eaat2,Glt1	1.91	0.93	6E-08	14.68870554	7	74	78	62.0	Excitatory amino acid transporter 2	Mus musculus
Q91YD3	Dcp1a,Mitc1,Smif	1.84	0.88	8E-06	16.09537065	5	35	36	65.2	mRNA-decapping enzyme 1A	Mus musculus
Q80U59	Kiaa0232,D5Ertd579e	1.84	0.88	0.0003	2.889050761	1	5	7	154.8	Uncharacterized protein KIAA0232	Mus musculus
Q9ERG0	Lima1,D15Ertd366e,Eplin	1.84	0.88	2E-15	9.13743917	13	85	107	84.1	LIM domain and actin-binding protein 1	Mus musculus
E9Q7X6	Heg1	1.84	0.88	0.0114	20.94803598	1	8	8	141.9	Protein HEG homolog 1	Mus musculus
E9Q9R9	Dlg5	1.83	0.87	8E-05	16.89434867	4	24	28	214.4	Disks large homolog 5	Mus musculus
P20152	Vim	1.82	0.87	9E-21	8.634872678	24	176	200	53.7	Vimentin	Mus musculus
Q80YT7	Pde4dip,Kiaa0454	1.82	0.87	0.0182	21.31156426	1	7	7	250.6	Myomegalin	Mus musculus
Q62407	Speg,Apeg1,Kiaa1297	1.80	0.85	0.0014	24.3362335	5	38	38	354.3	Striated muscle-specific serine/threonine-protein kinase	Mus musculus
Q68FF0	Kiaa1841	1.80	0.85	0.0344	33.66485982	2	15	16	82.0	Uncharacterized protein KIAA1841	Mus musculus
Q8BMB0	Emsy	1.80	0.85	0.0008	22.02227193	4	29	32	135.3	BRCA2-interacting transcriptional repressor EMSY	Mus musculus
Q9CXS4	Cenpv,Prr6	1.79	0.84	0.0016	24.69191084	5	39	43	27.5	Centromere protein V	Mus musculus
Q91VK1	Bzw2	1.79	0.84	0.0233	25.15202506	1	8	8	48.1	Basic leucine zipper and W2 domain-containing protein 2	Mus musculus
D3Z2H9	Tpm3-rs7	1.79	0.84	0.0048	14.85106281	1	7	8	29.0	Tropomyosin 3, related sequence 7	Mus musculus
Q5SXA9	Wwc1,Kiaa0869	1.78	0.83	7E-13	8.492669181	7	46	50	124.1	Protein KIBRA	Mus musculus
Q60634	Flot2,Esa1,M17s1	1.78	0.83	1E-19	8.340938211	15	125	145	47.0	Flotillin-2	Mus musculus
P51954	Nek1	1.78	0.83	0.0219	31.82296738	3	19	22	136.7	Serine/threonine-protein kinase Nek1	Mus musculus
Q8CI32	Bag5	1.76	0.82	0.017	17.82882101	1	6	8	50.9	BAG family molecular chaperone regulator 5	Mus musculus
Q5F4S9	Trpm3	1.75	0.81	0.0382	28.7906339	1	8	8	196.3	Transient receptor potential cation channel, subfamily M, member 3	Mus musculus
Q6PHZ8	Kcnip4,Calp,Kchip4	1.74	0.80	0.0115	23.95225986	2	11	11	28.8	Kv channel-interacting protein 4	Mus musculus
Q9WVJ5	Crybb1	1.74	0.80	0.0042	23.49681521	2	16	16	28.0	Beta-crystallin B1	Mus musculus
Q8K097	Faim2,Kiaa0950,Lfg,Lfg2,Nmp35	1.71	0.78	0.0164	30.5013515	2	20	21	35.3	Protein lifeguard 2	Mus musculus
Q9JLV1	Bag3,Bis,MNCb-2243	1.71	0.77	0.0221	24.74634672	1	8	8	61.9	BAG family molecular chaperone regulator 3	Mus musculus
B9EKR1	Ptprz1	1.69	0.76	3E-05	17.95247664	3	40	43	254.4	Receptor-type tyrosine-protein phosphatase zeta	Mus musculus
Q80TN4	Dnajc16,Kiaa0962	1.69	0.75	0.0383	34.91574117	1	16	16	89.1	DnaJ homolog subfamily C member 16	Mus musculus
Q60931	Vdac3	1.69	0.75	2E-05	19.36404898	10	75	80	30.8	Voltage-dependent anion-selective channel protein 3	Mus musculus
Q8C7U1	N4bp3	1.67	0.74	0.0002	18.27906212	2	22	24	60.0	NEDD4-binding protein 3	Mus musculus
Q921M4	Golga2	1.67	0.74	3E-05	15.0911013	3	22	24	113.3	Golgin subfamily A member 2	Mus musculus
Q6URW6	**Myh14**	**1.66**	**0.73**	**4E-10**	**11.95723492**	**8**	**65**	**71**	**228.6**	**Myosin-14**	**Mus musculus**
Q9ET43	Cldn12	1.65	0.72	0.0002	15.81540082	2	16	17	27.0	Claudin-12	Mus musculus
Q2KN98	Specc1l,Cytsa,Kiaa0376	1.64	0.71	1E-13	9.661421689	8	72	80	124.5	Cytospin-A	Mus musculus
Q01815	Cacna1c,Cach2,Cacn2,Cacnl1a1,Cchl1a1	1.63	0.70	0.0002	16.0361501	2	16	16	240.1	Voltage-dependent L-type calcium channel subunit alpha-1C	Mus musculus
Q60952	Cep250,Cep2,Inmp	1.63	0.70	0.0039	21.31448712	2	13	15	276.8	Centrosome-associated protein CEP250	Mus musculus
Q99JY8	Plpp3,Lpp3,Ppap2b	1.62	0.70	7E-09	10.73715204	3	34	38	35.2	Phospholipid phosphatase 3	Mus musculus
Q9DCZ4	Apoo,Fam121b,Mic23,Mic26	1.62	0.69	0.0225	29.60074467	2	13	14	22.6	MICOS complex subunit Mic26	Mus musculus
Q8JZP9	Gas2l1	1.62	0.69	0.002	20.63275648	2	15	16	72.4	GAS2-like protein 1	Mus musculus
Q9JJV5	Cacng3	1.61	0.69	9E-14	9.897722375	9	81	95	35.5	Voltage-dependent calcium channel gamma-3 subunit	Mus musculus
Q3UGS4	Mcrip1,Fam195b	1.61	0.69	0.0056	15.45144941	1	7	8	11.1	Mapk-regulated corepressor-interacting protein 1	Mus musculus
Q99LJ0	Cttnbp2nl,Kiaa1433	1.61	0.68	0.0006	19.51427496	3	20	22	69.8	CTTNBP2 N-terminal-like protein	Mus musculus
Q08917	Flot1	1.60	0.68	1E-19	8.218862381	16	117	137	47.5	Flotillin-1	Mus musculus
Q3UH68	Limch1,Kiaa1102	1.60	0.67	3E-18	7.542224441	11	75	88	118.2	LIM and calponin homology domains-containing protein 1	Mus musculus
Q5F2E8	Taok1,Kiaa1361	1.59	0.67	0.0498	25.97215694	1	6	8	116.0	Serine/threonine-protein kinase TAO1	Mus musculus
P70248	Myo1f	1.59	0.66	0.0007	17.90930686	2	15	16	125.9	Unconventional myosin-If	Mus musculus
Q8BSM7	Slc43a1,Lat3	1.58	0.66	0.0035	15.89518801	1	8	8	62.6	Large neutral amino acids transporter small subunit 3	Mus musculus
Q924S8	Spred1	1.58	0.66	0.0153	20.28560223	1	7	8	50.7	Sprouty-related, EVH1 domain-containing protein 1	Mus musculus
Q9QWW1	Homer2,Vesl2	1.56	0.64	1E-09	11.05820736	5	43	48	40.6	Homer protein homolog 2	Mus musculus
Q3UJB9	Edc4	1.56	0.64	0.0002	20.07095831	6	34	41	152.5	Enhancer of mRNA-decapping protein 4	Mus musculus
Q9EQN3	Tsc22d4,Thg1pit,Tilz2	1.56	0.64	0.0105	20.53718162	1	8	8	40.0	TSC22 domain family protein 4	Mus musculus
Q70FJ1	Akap9,Kiaa0803	1.55	0.64	0.0069	28.26761036	4	29	32	436.2	A-kinase anchor protein 9	Mus musculus
P51655	Gpc4	1.55	0.64	0.0003	7.422798252	1	7	8	62.6	Glypican-4	Mus musculus
Q8BJ37	Tdp1	1.55	0.64	0.043	29.73417665	1	8	8	68.7	RecName: Full=Tyrosyl-DNA phosphodiesterase 1; Short=Tyr-DNA phosphodiesterase 1; EC=3.1.4.-; AltName: Full=Protein expressed in male leptotene and zygotene spermatocytes 501; Short=MLZ-501	Mus musculus
Q04750	Top1,Top-1	1.55	0.63	0.0088	28.13160409	3	22	24	90.9	DNA topoisomerase 1	Mus musculus
Q8CGU1	Calcoco1,CocoA,Kiaa1536	1.55	0.63	0.0375	34.76419328	2	16	16	77.3	Calcium-binding and coiled-coil domain-containing protein 1	Mus musculus
B5TVM2	Ildr2,D1Ertd471e,Ll	1.53	0.62	3E-19	8.855401825	18	151	171	73.2	Immunoglobulin-like domain-containing receptor 2	Mus musculus
E9Q774	Akap11	1.53	0.61	0.0055	24.42360369	2	16	17	208.8	A kinase (PRKA) anchor protein 11	Mus musculus
Q8BUV6	Lsm11	1.52	0.60	0.0059	26.97976994	3	25	29	39.9	U7 snRNA-associated Sm-like protein LSm11	Mus musculus
Q61321	Six4,Arec3	1.52	0.60	0.0472	28.47663994	1	7	7	82.3	Homeobox protein SIX4	Mus musculus
Q9Z140	Cpne6	1.52	0.60	0.0053	27.27761069	4	29	33	61.8	Copine-6	Mus musculus
Q8BJF9	Chmp2b	1.51	0.60	0.0004	21.19855737	5	33	39	23.9	Charged multivesicular body protein 2b	Mus musculus
Q80TM6	R3hdm2,Kiaa1002	1.51	0.59	0.0152	30.86163387	3	23	24	114.6	R3H domain-containing protein 2	Mus musculus
P48193	Epb41,Epb4.1,Kiaa4056	1.51	0.59	3E-06	15.97340665	5	43	48	95.9	Protein 4.1	Mus musculus
E9QAT4	Sec16a,Kiaa0310,Sec16	1.50	0.59	1E-04	19.49573726	6	40	54	254.2	Protein transport protein Sec16A	Mus musculus
Q5U4C1	Gprasp1,Kiaa0443	1.50	0.58	7E-07	14.38935363	6	40	46	151.7	G-protein coupled receptor-associated sorting protein 1	Mus musculus
P48758	Cbr1,Cbr	0.67	-0.59	0.0144	30.34956372	2	22	25	30.6	Carbonyl reductase [NADPH] 1	Mus musculus
Q62523	Zyx	0.67	-0.59	0.0027	25.16543594	4	29	31	60.5	Zyxin	Mus musculus
Q9QZB7	Actr10,Act11,Actr11,Arp11	0.67	-0.59	0.0274	24.15160437	1	7	8	46.2	Actin-related protein 10	Mus musculus
Q5EE38	Acd	0.66	-0.59	0.0019	11.83915636	1	7	8	44.7	Adrenocortical dysplasia protein	Mus musculus
Q08529	Capn2	0.66	-0.59	0.0248	32.3533311	3	18	22	79.9	Calpain-2 catalytic subunit	Mus musculus
P28660	Nckap1,Hem2,Kiaa0587,Nap1	0.66	-0.59	0.0023	18.73901819	2	12	16	128.8	Nck-associated protein 1	Mus musculus
O35683	Ndufa1	0.66	-0.59	0.0017	20.79051728	2	16	16	8.1	NADH dehydrogenase [ubiquinone] 1 alpha subcomplex subunit 1	Mus musculus
Q9CWF2	Tubb2b	0.66	-0.59	0.0036	25.99649015	2	29	29	50.0	Tubulin beta-2B chain	Mus musculus
P28738	Kif5c,Nkhc2	0.66	-0.59	2E-12	9.854919303	7	59	64	109.3	Kinesin heavy chain isoform 5C	Mus musculus

Q9JIS5	Sv2a,Kiaa0736,Sv2	0.66	-0.60	1E-05	16.49127257	6	36	47	82.6	Synaptic vesicle glycoprotein 2A	Mus musculus
Q9Z0Y1	Dctn3	0.66	-0.60	0.0446	37.32886229	3	21	24	21.0	Dynactin subunit 3	Mus musculus
Q791T5	Mtch1	0.66	-0.60	0.0031	21.28063227	2	14	17	41.6	Mitochondrial carrier homolog 1	Mus musculus
Q9QYR6	Map1a,Mtap1,Mtap1a	0.66	-0.60	5E-89	4.164991746	80	779	891	300.1	Microtubule-associated protein 1A	Mus musculus
Q9CZD3	Gars	0.66	-0.60	0.004	16.40472004	1	8	8	81.9	Glycine--tRNA ligase	Mus musculus
Q8CBY8	Dctn4	0.66	-0.60	0.0057	24.58410111	3	17	21	53.1	Dynactin subunit 4	Mus musculus
P99024	Tubb5	0.66	-0.60	1E-16	8.994813297	10	98	116	49.7	Tubulin beta-5 chain	Mus musculus
Q8K1M6	Dnm1l,Drp1	0.66	-0.60	1E-09	12.75243318	10	74	86	82.7	Dynamin-1-like protein	Mus musculus
Q5EBJ4	Ermn,Kiaa1189	0.66	-0.60	0.004	21.36222955	2	13	16	32.1	Ermin	Mus musculus
O54916	Reps1	0.66	-0.61	0.0499	35.53319061	2	13	13	86.5	RalBP1-associated Eps domain-containing protein 1	Mus musculus
Q8R0A7	Kiaa0513	0.66	-0.61	5E-08	12.22193906	5	36	42	46.3	Uncharacterized protein KIAA0513	Mus musculus
Q9WUA3	Pfkp,Pfkc	0.66	-0.61	3E-17	8.883185891	13	107	127	85.5	ATP-dependent 6-phosphofructokinase, platelet type	Mus musculus
P35486	Pdha1,Pdha-1	0.66	-0.61	0.0002	19.22573496	4	29	33	43.2	Pyruvate dehydrogenase E1 component subunit alpha, somatic form, mitochondrial	Mus musculus
Q8R191	Syngr3	0.65	-0.61	0.0027	12.80367486	1	7	8	24.6	Synaptogyrin-3	Mus musculus
Q9D1F4	Akt1s1 {ECO:0000312|MGI:MGI:1914854	0.65	-0.61	0.0095	28.16343782	3	21	22	27.5	Proline-rich AKT1 substrate 1	Mus musculus
Q9DBG3	Ap2b1,Clapb1	0.65	-0.61	5E-07	12.27665765	3	27	32	104.6	AP-2 complex subunit beta	Mus musculus
Q7TMY8	Huwe1,Kiaa0312,Ureb1	0.65	-0.61	0.0235	25.22582338	1	8	8	482.6	E3 ubiquitin-protein ligase HUWE1	Mus musculus
Q9D0I9	Rars	0.65	-0.61	0.0006	8.99994693	1	7	8	75.7	Arginine--tRNA ligase, cytoplasmic	Mus musculus
Q8VIJ6	Sfpq	0.65	-0.61	0.0024	24.6654712	4	28	32	75.4	Splicing factor, proline- and glutamine-rich	Mus musculus
Q6Y685	Tacc1	0.65	-0.62	0.0013	19.97484805	2	17	19	84.0	Transforming acidic coiled-coil-containing protein 1	Mus musculus
P62852	Rps25	0.65	-0.62	2E-05	18.38236126	7	54	56	13.7	40S ribosomal protein S25	Mus musculus
Q8R001	Mapre2	0.65	-0.62	0.0115	28.4244877	3	19	24	36.9	Microtubule-associated protein RP/EB family member 2	Mus musculus
P47857	Pfkm,Pfk-m,Pfka	0.65	-0.62	7E-23	8.0328783	14	173	190	85.3	ATP-dependent 6-phosphofructokinase, muscle type	Mus musculus
Q9CQD1	Rab5a,mnyRab5a	0.65	-0.62	0.0097	29.16190164	4	26	27	23.6	Ras-related protein Rab-5A	Mus musculus
P04264	KRT1,KRTA	0.65	-0.63	4E-09	14.5272373	19	151	167	66.0	SWISS-PROT:P04264 Tax_Id=9606 Gene_Symbol=KRT1 Keratin, type II cytoskeletal 1	Homo sapiens
O35643	Ap1b1,Adtb1	0.65	-0.63	5E-06	9.566031017	2	14	17	103.9	AP-1 complex subunit beta-1	Mus musculus
P61264	Stx1b,Stx1b1,Stx1b2	0.64	-0.63	0.0111	29.60131804	3	24	24	33.2	Syntaxin-1B	Mus musculus
Q9Z1G4	Atp6v0a1,Atp6n1	0.64	-0.63	2E-05	18.12694413	9	54	68	96.5	V-type proton ATPase 116 kDa subunit a isoform 1	Mus musculus
Q9D1G1	Rab1b	0.64	-0.63	1E-06	15.53166453	5	49	59	22.2	Ras-related protein Rab-1B	Mus musculus
Q9D6F9	Tubb4a,Tubb4	0.64	-0.64	8E-16	9.638276052	10	112	120	49.6	Tubulin beta-4A chain	Mus musculus
P63101	Ywhaz	0.64	-0.64	9E-07	15.24816876	5	46	50	27.8	14-3-3 protein zeta/delta	Mus musculus
O09111	Ndufb11,Np15	0.64	-0.64	0.0059	26.18282633	3	21	24	17.4	NADH dehydrogenase [ubiquinone] 1 beta subcomplex subunit 11, mitochondrial	Mus musculus
P0C7L0	Wipf3,Cr16	0.64	-0.64	0.0007	22.46339467	4	35	37	49.5	WAS/WASL-interacting protein family member 3	Mus musculus
Q64521	Gpd2,Gdm1	0.64	-0.64	0.0217	31.76778378	2	19	23	81.0	Glycerol-3-phosphate dehydrogenase, mitochondrial	Mus musculus
O08749	Dld	0.64	-0.64	1E-05	17.55817657	7	49	53	54.3	Dihydrolipoyl dehydrogenase, mitochondrial	Mus musculus
Q9WTQ5	Akap12,Gag12,Ssecks	0.64	-0.64	0.0215	32.96563539	3	24	24	180.7	A-kinase anchor protein 12	Mus musculus
P80318	Cct3,Cctg	0.64	-0.64	0.0031	24.3616954	4	23	26	60.6	T-complex protein 1 subunit gamma	Mus musculus
Q3TDD9	Ppp1r21,Cedc128,Klraq1	0.64	-0.64	0.0079	29.06439763	3	31	32	88.3	Protein phosphatase 1 regulatory subunit 21	Mus musculus
Q8K0T0	Rtn1,Nsp	0.64	-0.65	9E-10	12.84892757	9	82	93	83.6	Reticulon-1	Mus musculus
Q9WVK4	Ehd1,Past1	0.64	-0.65	0.0002	18.9926849	2	24	24	60.6	EH domain-containing protein 1	Mus musculus
O88741	Gdap1	0.64	-0.65	5E-08	12.94116473	6	44	53	41.3	Ganglioside-induced differentiation-associated protein 1	Mus musculus
Q3UH60	Dip2b,Kiaa1463	0.64	-0.65	0.0055	25.24688507	3	19	19	171.1	Disco-interacting protein 2 homolog B	Mus musculus
Q9CR61	Ndufb7	0.64	-0.65	0.0078	19.13782391	1	8	9	16.3	NADH dehydrogenase [ubiquinone] 1 beta subcomplex subunit 7	Mus musculus
Q9EQF6	Dpysl5,Crmp5	0.64	-0.65	5E-05	19.29334809	5	50	60	61.5	Dihydropyrimidinase-related protein 5	Mus musculus
Q9QXY6	Ehd3,Ehd2	0.63	-0.66	0.0017	20.79487866	2	16	16	60.8	EH domain-containing protein 3	Mus musculus
A8DUK4	Hbb-b1,Hbb-b2,Hbbt1,Hbbt2	0.63	-0.66	0.0351	36.67390913	5	29	35	15.7	Beta-globin	Mus musculus
Q6GYP7	Ralgapa1,Garnl1,Kiaa0884,Tulip1	0.63	-0.66	9E-10	11.35388119	7	50	60	229.4	Ral GTPase-activating protein subunit alpha-1	Mus musculus
Q8BW74	Hlf	0.63	-0.66	0.0167	17.70383814	1	6	8	33.1	Hepatic leukemia factor	Mus musculus
P17182	Eno1,Eno-1	0.63	-0.66	8E-05	16.97164972	2	23	24	47.1	Alpha-enolase	Mus musculus
P97427	Crmp1,Dpysl1,Ulip3	0.63	-0.66	2E-10	12.29460088	13	86	98	62.2	Dihydropyrimidinase-related protein 1	Mus musculus
Q3UGY8	Arfgef3,Big3,D10Bwg1379e,Kiaa1244	0.63	-0.66	0.0003	21.38739924	7	41	46	240.1	Brefeldin A-inhibited guanine nucleotide-exchange protein 3	Mus musculus
Q6ZQK5	Acap2,Centb2,Kiaa0041	0.63	-0.66	0.0008	17.43091707	2	14	16	87.2	Arf-GAP with coiled-coil, ANK repeat and PH domain-containing protein 2	Mus musculus
Q9D5V5	Cul5	0.63	-0.67	0.0168	17.74380188	1	6	6	91.0	Cullin-5	Mus musculus
Q8BYK5	Phactr3,Scapin1	0.63	-0.67	0.0003	17.5508534	3	18	21	62.7	Phosphatase and actin regulator 3	Mus musculus
Q922B1	Macrod1,Lrp16	0.63	-0.67	0.0356	26.10912592	1	7	8	35.3	O-acetyl-ADP-ribose deacetylase MACROD1	Mus musculus
Q9JK48	Sh3glb1,Kiaa0491	0.63	-0.67	0.0046	16.90829842	2	9	10	40.9	Endophilin-B1	Mus musculus
Q8R3V5	Sh3glb2,Kiaa1848	0.63	-0.67	8E-06	15.27177455	4	29	31	44.5	Endophilin-B2	Mus musculus
P19783	Cox4i1,Cox4,Cox4a	0.63	-0.68	5E-05	20.27259545	7	69	76	19.5	Cytochrome c oxidase subunit 4 isoform 1, mitochondrial	Mus musculus
O35250	Exoc7,Exo70	0.63	-0.68	5E-05	18.14492564	5	34	38	80.0	Exocyst complex component 7	Mus musculus
P62631	Eef1a2,Eef1al,Stn	0.62	-0.68	1E-08	12.9158935	8	54	59	50.5	Elongation factor 1-alpha 2	Mus musculus
P56399	Usp5,Isot	0.62	-0.68	2E-05	17.21876796	4	37	40	95.8	Ubiquitin carboxyl-terminal hydrolase 5	Mus musculus
Q8R313	Exoc6,Sec15a,Sec15l1	0.62	-0.69	0.0199	24.0868969	1	8	8	93.1	Exocyst complex component 6	Mus musculus
Q8K394	Plcl2,Kiaa1092,Plce2	0.62	-0.69	0.0082	26.10152014	3	17	18	125.8	Inactive phospholipase C-like protein 2	Mus musculus
A0A338P6R8	Gm49601	0.62	-0.69	0.0003	18.92192299	2	23	24	41.9	Uncharacterized protein	Mus musculus
Q6PDL0	Dync1li2,Dncli2,Dnclic2	0.62	-0.69	3E-11	10.89446372	10	66	82	54.2	Cytoplasmic dynein 1 light intermediate chain 2	Mus musculus
Q9JJR9	Nrip3,D7H11orf14	0.62	-0.69	0.0095	26.18782392	1	15	16	26.9	Nuclear receptor-interacting protein 3	Mus musculus
Q8BRK8	Prkaa2	0.62	-0.69	0.0327	27.58059041	1	8	8	62.0	5'-AMP-activated protein kinase catalytic subunit alpha-2	Mus musculus
Q62448	Eif4g2,Nat1	0.62	-0.70	6E-06	12.71447309	3	20	28	102.1	Eukaryotic translation initiation factor 4 gamma 2	Mus musculus
Q8BVE3	Atp6v1h	0.62	-0.70	1E-10	12.47752868	10	95	106	55.9	V-type proton ATPase subunit H	Mus musculus
O35382	Exoc4,Sec8,Sec8l1	0.62	-0.70	2E-05	13.23828219	4	19	27	110.5	Exocyst complex component 4	Mus musculus
O54781	Srpk2	0.62	-0.70	0.0329	33.35093807	2	15	16	76.8	SRSF protein kinase 2	Mus musculus
Q3TCJ1	Fam175b,Abro1,Kiaa0157	0.61	-0.70	0.0003	18.27332797	2	21	22	46.9	BRISC complex subunit Abraxas 2	Mus musculus
Q8VDN2	Atp1a1	0.61	-0.71	9E-16	9.516212306	14	106	117	113.0	Sodium/potassium-transporting ATPase subunit alpha-1	Mus musculus
C8YR32	Loxhd1	0.61	-0.71	0.0332	25.5151337	1	7	8	235.8	Lipoxygenase homology domain-containing protein 1	Mus musculus
Q80UJ7	Rab3gap1,Kiaa0066,Rab3gap	0.61	-0.71	8E-05	16.90205191	4	24	29	110.2	Rab3 GTPase-activating protein catalytic subunit	Mus musculus
Q9CZS1	Aldh1b1,Aldhx	0.61	-0.71	0.0454	30.21256766	1	8	8	57.6	Aldehyde dehydrogenase X, mitochondrial	Mus musculus
Q61644	Pacsin1,Pacsin	0.61	-0.71	2E-05	18.16503736	6	47	57	50.6	Protein kinase C and casein kinase substrate in neurons protein 1	Mus musculus
P28661	Sept4,Pnutl2	0.61	-0.71	0.0029	25.62759717	4	31	31	54.9	Septin-4	Mus musculus
Q8CHC4	Synj1,Kiaa0910	0.61	-0.72	2E-33	6.22544737	26	196	219	172.6	Synaptojanin-1	Mus musculus
O35926	Cdk5r2,Nck5ai	0.61	-0.72	0.0453	25.01776074	1	6	8	38.9	Cyclin-dependent kinase 5 activator 2	Mus musculus
P62814	Atp6v1b2,Atp6b2,Vat2	0.61	-0.72	1E-18	8.41475145	13	109	121	56.6	V-type proton ATPase subunit B, brain isoform	Mus musculus
Q8JZQ9	Eif3b,Eif3s9	0.60	-0.73	0.0069	13.27849751	1	6	8	91.4	Eukaryotic translation initiation factor 3 subunit B	Mus musculus
Q8CB44	Gramd4,Dip,Kiaa0767	0.60	-0.73	0.0231	25.10031497	1	8	8	72.3	GRAM domain-containing protein 4	Mus musculus
Q80UG5	Sept9,Kiaa0991,Sint1	0.60	-0.73	2E-18	8.127504836	11	92	98	65.6	Septin-9	Mus musculus
P11983	Tcp1,Cct1,Ccta	0.60	-0.74	2E-15	8.972704051	11	80	87	60.4	T-complex protein 1 subunit alpha	Mus musculus
Q62167	Ddx3x,D1Pas1-rs2,Ddx3,Dead3,Erh	0.60	-0.74	5E-11	10.91785697	10	62	71	73.1	ATP-dependent RNA helicase DDX3X	Mus musculus
P13645	KRT10,KPP	0.60	-0.75	0.0088	30.34321092	7	44	56	59.5	SWISS-PROT:P13645 Tax_Id=9606 Gene_Symbol=KRT10 Keratin, type I cytoskeletal 10	Homo sapiens
P19096	Fasn	0.60	-0.75	0.0002	18.10114002	4	24	25	272.4	Fatty acid synthase	Mus musculus
Q6PCN3	Ttbk1	0.60	-0.75	0.0013	23.56332909	5	32	38	141.6	Tau-tubulin kinase 1	Mus musculus
P63040	Cplx1	0.60	-0.75	0.001	19.35733809	2	16	16	15.1	Complexin-1	Mus musculus
P80316	Cct5,Ccte,Kiaa0098	0.60	-0.75	9E-07	15.10554271	5	45	48	59.6	T-complex protein 1 subunit epsilon	Mus musculus
P47809	Map2k4,Jnkk1,Mek4,Mkk4,Prkmk4,Sek1,	0.60	-0.75	4E-07	14.93521097	6	51	54	44.1	Dual specificity mitogen-activated protein kinase kinase 4	Mus musculus
O88485	Dync1i1,Dnci1,Dncic1	0.59	-0.75	7E-09	12.58717776	6	53	60	70.7	Cytoplasmic dynein 1 intermediate chain 1	Mus musculus
Q8BWJ3	Phka2	0.59	-0.76	0.0293	26.78871653	1	8	8	138.5	Phosphorylase b kinase regulatory subunit alpha, liver isoform	Mus musculus
Q68FL4	Ahcyl2	0.59	-0.76	0.0105	20.51269916	1	8	8	66.9	Putative adenosylhomocysteinase 3	Mus musculus
Q9ERD7	Tubb3	0.59	-0.76	2E-26	7.496062752	16	200	220	50.4	Tubulin beta-3 chain	Mus musculus
Q0GNC1	Inf2	0.59	-0.76	0.0446	30.04891962	1	8	8	138.6	Inverted formin-2	Mus musculus
Q99KJ8	Dctn2	0.58	-0.78	1E-29	6.541067989	18	169	189	44.1	Dynactin subunit 2	Mus musculus
P63038	Hspd1,Hsp60	0.58	-0.78	5E-18	9.442267052	20	164	180	61.0	60 kDa heat shock protein, mitochondrial	Mus musculus
P54775	Psmc4,Tbp7	0.58	-0.78	6E-10	10.42750198	7	42	50	47.4	26S proteasome regulatory subunit 6B	Mus musculus
Q9CZC8	Scrn1,Kiaa0193	0.58	-0.79	0.0007	20.8395091	2	23	24	46.3	Secernin-1	Mus musculus
P11499	Hsp90ab1,Hsp84,Hsp84-1,Hspcb	0.58	-0.79	4E-06	13.28309243	4	24	27	83.3	Heat shock protein HSP 90-beta	Mus musculus
O54774	Ap3d1,Ap3d	0.58	-0.80	7E-05	19.29308191	6	43	51	135.1	AP-3 complex subunit delta-1	Mus musculus
Q9WUM5	Suclg1	0.58	-0.80	1E-29	5.550741917	13	108	128	36.2	Succinate--CoA ligase [ADP/GDP-forming] subunit alpha, mitochondrial	Mus musculus
P42859	Htt,Hd,Hdh	0.58	-0.80	0.0025	19.92755744	3	14	22	344.7	Huntingtin	Mus musculus
Q9R0P9	Uchl1	0.57	-0.80	1E-06	12.74086231	3	26	31	24.8	Ubiquitin carboxyl-terminal hydrolase isozyme L1	Mus musculus
P16330	Cnp,Cnp1	0.57	-0.80	3E-16	9.811805488	15	135	144	47.1	2',3'-cyclic-nucleotide 3'-phosphodiesterase	Mus musculus
Q6PB70	Ano8,Kiaa1623,Tmem16h	0.57	-0.81	0.0023	21.62641507	2	16	16	119.1	Anoctamin-8	Mus musculus
Q8BGT1	Flrt3,Kiaa1469	0.57	-0.81	0.0014	4.963691556	1	5	7	72.9	Leucine-rich repeat transmembrane protein FLRT3	Mus musculus
P70336	**Rock2**	**0.57**	**-0.81**	**9E-13**	**9.440778125**	**7**	**57**	**63**	**160.6**	**Rho-associated protein kinase 2**	**Mus musculus**
O89053	Coro1a,Coro1	0.57	-0.81	0.0018	22.14337354	3	20	20	51.0	Coronin-1A	Mus musculus
Q91VA7	Idh3b,mCG_9915	0.57	-0.82	4E-22	6.66701991	11	88	108	42.2	Isocitrate dehydrogenase [NAD] subunit, mitochondrial	Mus musculus
Q8CBW3	Abi1,Ssh3bp1	0.57	-0.82	0.001	22.95091248	4	32	37	52.3	Abl interactor 1	Mus musculus
Q91YD9	Wasl	0.57	-0.82	9E-05	16.41404421	2	21	24	54.3	Neural Wiskott-Aldrich syndrome protein	Mus musculus

Q05920	Pc,Pcx	0.56	-0.83	5E-05	13.8504378	3	17	23	129.7	Pyruvate carboxylase, mitochondrial	Mus musculus
Q9Z2Q6	Sept5,Pnutl1	0.56	-0.83	0.0021	20.7624795	1	15	16	42.7	Septin-5	Mus musculus
Q9Z0E0	Ncdn,Kiaa0607,Sfap75	0.56	-0.83	3E-07	12.99659918	4	33	39	78.9	Neurochondrin	Mus musculus
P97452	Bop1,Kiaa0124	0.56	-0.83	0.0235	23.04880837	1	7	7	82.5	Ribosome biogenesis protein BOP1	Mus musculus
Q91XU3	Pip4k2c,Pip5k2c	0.56	-0.83	0.0078	22.11925412	2	11	13	47.3	Phosphatidylinositol 5-phosphate 4-kinase type-2 gamma	Mus musculus
Q8CDG3	Vcpip1,Vcip135	0.56	-0.83	6E-05	17.79309022	4	30	32	134.5	Deubiquitinating protein VCIP135	Mus musculus
Q8BH59	Slc25a12,Aralar1	0.56	-0.84	3E-22	6.808851372	10	92	109	74.6	Calcium-binding mitochondrial carrier protein Aralar1	Mus musculus
Q9QYF9	Ndrg3,Ndr3	0.56	-0.84	0.0003	17.37774774	2	18	23	41.6	Protein NDRG3	Mus musculus
Q9CZ13	Uqcrc1	0.56	-0.84	0.0457	33.94465964	3	13	16	52.9	Cytochrome b-c1 complex subunit 1, mitochondrial	Mus musculus
Q7TQD2	Tppp	0.56	-0.84	5E-19	7.892112687	13	95	114	23.6	Tubulin polymerization-promoting protein	Mus musculus
P97441	Slc30a3,Znt3	0.56	-0.84	0.0215	22.35798666	1	7	8	41.8	Zinc transporter 3	Mus musculus
O08788	Dctn1	0.55	-0.85	4E-36	5.419551124	18	157	186	141.7	Dynactin subunit 1	Mus musculus
A2AGT5	Ckap5	0.55	-0.85	2E-17	8.398294525	13	90	103	225.6	Cytoskeleton-associated protein 5	Mus musculus
Q76MZ3	Ppp2r1a	0.55	-0.85	9E-11	9.25244293	7	39	48	65.3	Serine/threonine-protein phosphatase 2A 65 kDa regulatory subunit A alpha isoform	Mus musculus
P32921	Wars,Wrs	0.55	-0.86	0.0063	23.8282644	2	14	16	54.4	Tryptophan--tRNA ligase, cytoplasmic	Mus musculus
Q3TXS7	Psmd1	0.55	-0.86	0.0053	23.76258668	3	16	19	105.7	26S proteasome non-ATPase regulatory subunit 1	Mus musculus
P68372	Tubb4b,Tubb2c	0.55	-0.87	2E-15	9.124449919	7	82	90	49.8	Tubulin beta-4B chain	Mus musculus
A6H5Z3	Exoc6b,Sec15b,Sec15l2	0.55	-0.87	6E-11	10.06208496	7	47	54	94.1	Exocyst complex component 6B	Mus musculus
Q8BH57	Wdr48,Kiaa1449,Uaf1	0.55	-0.87	0.0023	23.22394748	2	21	21	76.0	WD repeat-containing protein 48	Mus musculus
O35098	Dpysl4,Crmp3,Ulip4	0.54	-0.88	8E-07	15.09470053	7	48	55	62.0	Dihydropyrimidinase-related protein 4	Mus musculus
Q3TPX4	Exoc5,Sec10l1	0.54	-0.89	9E-05	14.7032294	2	16	16	81.7	Exocyst complex component 5	Mus musculus
P46471	Psmc2,Mss1	0.54	-0.89	0.0003	16.81645404	1	16	16	48.6	26S proteasome regulatory subunit 7	Mus musculus
Q7TPD0	Ints3	0.54	-0.89	0.0002	7.080689449	1	7	8	117.9	Integrator complex subunit 3	Mus musculus
Q9Z1Z0	Uso1,Vdp	0.54	-0.90	0.0235	23.01956622	1	7	7	107.0	General vesicular transport factor p115	Mus musculus
Q8BGQ1	Vipas39,Spe39,Vipar	0.54	-0.90	0.0027	20.15999544	2	13	17	56.6	Spermatogenesis-defective protein 39 homolog	Mus musculus
Q7TMM9	Tubb2a,Tubb2	0.53	-0.91	4E-14	8.346312628	5	54	64	49.9	Tubulin beta-2A chain	Mus musculus
Q9CR62	Slc25a11	0.53	-0.91	2E-05	17.94373952	5	42	44	34.2	Mitochondrial 2-oxoglutarate/malate carrier protein	Mus musculus
P13707	Gpd1,Gdc-1,Gdc1,Kiaa4010	0.53	-0.91	0.0232	22.93560675	1	7	8	37.6	Glycerol-3-phosphate dehydrogenase [NAD(+)], cytoplasmic	Mus musculus
Q8C3K6	Slc5a1	0.53	-0.92	0.0345	27.99532286	1	8	8	73.4	Sodium/glucose cotransporter 1	Mus musculus
P31938	Map2k1,Mek1,Prkmk1	0.53	-0.92	6E-09	8.889779755	4	25	28	43.5	Dual specificity mitogen-activated protein kinase kinase 1	Mus musculus
Q91WD5	Ndufs2	0.53	-0.92	0.0221	24.77984025	1	8	12	52.6	NADH dehydrogenase [ubiquinone] iron-sulfur protein 2, mitochondrial	Mus musculus
Q80UM3	Naa15,Narg1,Nat1,Tbdn-1,Tubedown	0.53	-0.93	0.0068	18.43638905	1	8	8	101.0	N-alpha-acetyltransferase 15, NatA auxiliary subunit	Mus musculus
Q60676	Ppp5c	0.53	-0.93	0.0185	23.62100568	1	8	8	56.9	Serine/threonine-protein phosphatase 5	Mus musculus
Q9Z2V5	Hdac6	0.53	-0.93	0.0284	30.37954409	2	12	18	125.8	Histone deacetylase 6	Mus musculus
P60670	Nploc4,Kiaa1499,Npl4	0.52	-0.93	0.0284	21.30846203	1	6	6	68.0	Nuclear protein localization protein 4 homolog	Mus musculus
Q9QXK3	Copg2	0.52	-0.93	0.0413	24.20678602	1	6	8	97.7	Coatomer subunit gamma-2	Mus musculus
Q9DB60	Fam213b	0.52	-0.94	0.0345	28.00063586	1	8	8	21.7	Prostamide/prostaglandin F synthase	Mus musculus
Q8C1B7	Sept11,D5Ertd606e	0.52	-0.94	3E-11	8.802837108	5	37	40	49.7	Septin-11	Mus musculus
P68368	Tuba4a,Tuba4	0.52	-0.94	3E-20	8.202020514	12	127	143	49.9	Tubulin alpha-4A chain	Mus musculus
P99028	Uqcrh	0.51	-0.96	0.0002	7.14842087	1	7	8	10.4	Cytochrome b-c1 complex subunit 6, mitochondrial	Mus musculus
O08553	Dpysl2,Crmp2,Ulip2	0.51	-0.96	7E-49	4.677151465	29	214	253	62.3	Dihydropyrimidinase-related protein 2	Mus musculus
Q9DCJ5	Ndufa8	0.51	-0.97	3E-17	8.46770011	7	89	100	20.0	NADH dehydrogenase [ubiquinone] 1 alpha subcomplex subunit 8	Mus musculus
P05064	Aldoa,Aldo1	0.51	-0.98	0.0058	17.81431718	2	9	11	39.4	Fructose-bisphosphate aldolase A	Mus musculus
O08599	Stxbp1	0.51	-0.98	9E-38	5.828061239	24	216	237	67.6	Syntaxin-binding protein 1	Mus musculus
Q9CQ54	Ndufc2	0.51	-0.98	8E-09	10.49925756	4	32	39	14.2	NADH dehydrogenase [ubiquinone] 1 subunit C2	Mus musculus
P23116	Eif3a,Csma,Eif3,Eif3s10	0.50	-0.99	9E-07	14.46573521	6	39	43	161.9	Eukaryotic translation initiation factor 3 subunit A	Mus musculus
Q8VCM4	Lipt1	0.50	-0.99	0.0021	12.05548518	1	7	8	42.1	Lipoyltransferase 1, mitochondrial	Mus musculus
Q9Z1S5	Sept3,Sep3	0.50	-1.00	0.0002	6.68502137	1	7	8	40.0	Neuronal-specific septin-3	Mus musculus
Q6PGL7	Fam21,D6Wsu116e,Kiaa0592	0.50	-1.00	7E-07	13.41536004	4	32	37	145.3	WASH complex subunit 2	Mus musculus
Q8BH66	Atl1,Spg3a	0.50	-1.00	6E-06	14.76347878	4	28	31	63.4	Atlastin-1	Mus musculus
Q99JR1	Sfxn1,F	0.50	-1.00	0.0242	25.45033434	1	8	8	35.6	Sideroflexin-1	Mus musculus
P62192	Psmc1	0.50	-1.01	2E-17	7.722487515	11	72	82	49.2	26S proteasome regulatory subunit 4	Mus musculus
Q8R366	Igsf8,Ewi2,Ket4,Pgrl	0.50	-1.01	0.0492	28.87179353	1	7	7	65.0	Immunoglobulin superfamily member 8	Mus musculus
Q99JP0	Map4k3	0.49	-1.02	0.0072	25.55208399	2	16	16	101.1	Mitogen-activated protein kinase kinase kinase kinase 3	Mus musculus
Q9JKY5	Hip1r	0.49	-1.02	4E-09	8.640175282	4	25	26	119.4	Huntingtin-interacting protein 1-related protein	Mus musculus
O55125	Nipsnap1	0.49	-1.03	6E-05	12.88180723	2	14	15	33.4	Protein NipSnap homolog 1	Mus musculus
Q9DBP5	Cmpk1,Cmk,Cmpk,Uck,Umk,Umpk	0.49	-1.03	0.0151	25.34492994	2	11	12	22.2	UMP-CMP kinase	Mus musculus
Q9JME5	Ap3b2	0.49	-1.03	2E-12	9.861604817	7	59	63	119.2	AP-3 complex subunit beta-2	Mus musculus
Q8K2B3	Sdha	0.49	-1.03	2E-16	5.849849384	6	41	54	72.6	Succinate dehydrogenase [ubiquinone] flavoprotein subunit, mitochondrial	Mus musculus
Q9Z2I9	Sucla2	0.49	-1.03	3E-20	7.305515844	13	90	98	50.1	Succinate--CoA ligase [ADP-forming] subunit beta, mitochondrial	Mus musculus
Q80UP3	Dgkz	0.49	-1.04	0.0062	27.11724354	4	25	31	104.0	Diacylglycerol kinase zeta	Mus musculus
Q8QZT1	Acat1	0.48	-1.06	7E-14	8.587501822	9	57	70	44.8	Acetyl-CoA acetyltransferase, mitochondrial	Mus musculus
Q80TJ1	Cadps,Caps,Caps1,Kiaa1121	0.48	-1.07	8E-08	12.31475451	5	36	40	153.1	Calcium-dependent secretion activator 1	Mus musculus
Q9CQC7	Ndufb4	0.48	-1.07	8E-10	11.67225517	8	55	62	15.1	NADH dehydrogenase [ubiquinone] 1 beta subcomplex subunit 4	Mus musculus
Q9JHU4	Dync1h1,Dhc1,Dnch1,Dnchc1,Dyhc	0.48	-1.07	3E-52	4.826459936	39	280	346	532.0	Cytoplasmic dynein 1 heavy chain 1	Mus musculus
O55131	Sept7,Cdc10	0.47	-1.08	3E-18	6.512682631	6	56	61	50.5	Septin-7	Mus musculus
Q99KI0	Aco2	0.47	-1.08	1E-06	16.52980855	12	73	86	85.5	Aconitate hydratase, mitochondrial	Mus musculus
P62827	Ran,Rasl2-8	0.47	-1.09	2E-05	13.79563903	3	20	24	24.4	GTP-binding nuclear protein Ran	Mus musculus
O35143	Atpif1,Atpi,If1	0.47	-1.09	4E-05	15.98003199	3	23	24	12.2	ATPase inhibitor, mitochondrial	Mus musculus
P57746	Atp6v1d,Atp6m,Vatd	0.47	-1.09	6E-06	8.977145815	2	14	20	28.4	V-type proton ATPase subunit D	Mus musculus
Q91V61	Sfxn3	0.47	-1.10	5E-21	6.686427514	11	80	90	35.4	Sideroflexin-3	Mus musculus
Q91V92	Acly	0.46	-1.10	0.011	20.73857494	1	8	8	119.7	ATP-citrate synthase	Mus musculus
Q80VY9	Dhx33	0.46	-1.11	0.0076	18.98221241	1	8	8	78.3	Putative ATP-dependent RNA helicase DHX33	Mus musculus
Q9JIG7	Ccdc22,DXImx40e	0.46	-1.11	0.0128	24.44748484	1	11	11	70.8	Coiled-coil domain-containing protein 22	Mus musculus
Q148V7	Kiaa1468	0.46	-1.12	0.006	24.74947585	2	16	16	134.6	RAB11-binding protein RELCH	Mus musculus
Q91VD9	Ndufs1	0.46	-1.13	6E-09	9.859837859	4	29	32	79.8	NADH-ubiquinone oxidoreductase 75 kDa subunit, mitochondrial	Mus musculus
Q9D172	D10Jhu81e	0.45	-1.15	5E-05	12.44316736	2	14	22	28.1	Glutamine amidotransferase-like class 1 domain-containing protein 3A, mitochondrial	Mus musculus
Q9D6R2	Idh3a	0.45	-1.15	3E-05	12.28838062	2	15	16	39.6	Isocitrate dehydrogenase [NAD] subunit alpha, mitochondrial	Mus musculus
Q8QZY1	Eif3l,Eif3eip,Eif3s6ip,Paf67	0.45	-1.15	0.0012	15.84824927	2	11	14	66.6	Eukaryotic translation initiation factor 3 subunit L	Mus musculus
Q9DCT2	Ndufs3	0.45	-1.16	0.0002	14.67644467	2	14	16	30.1	NADH dehydrogenase [ubiquinone] iron-sulfur protein 3, mitochondrial	Mus musculus
P70404	Idh3g	0.45	-1.16	2E-13	6.909205943	6	36	44	42.8	Isocitrate dehydrogenase [NAD] subunit gamma 1, mitochondrial	Mus musculus
Q9EQH3	Vps35,Mem3	0.45	-1.17	0.0001	8.081625795	1	8	8	91.7	Vacuolar protein sorting-associated protein 35	Mus musculus
Q9WTM5	Ruvbl2	0.44	-1.17	0.007	18.61019626	1	8	8	51.1	RuvB-like 2	Mus musculus
Q9WTL7	Lypla2	0.44	-1.18	0.0484	30.80502895	1	8	8	24.8	Acyl-protein thioesterase 2	Mus musculus
E9Q7P1	Col22a1	0.44	-1.19	0.0467	30.48981953	1	8	8	159.9	Collagen, type XXII, alpha 1	Mus musculus
P10637	Mapt,Mtapt,Tau	0.43	-1.20	8E-85	3.143184771	32	281	351	76.2	Microtubule-associated protein tau	Mus musculus
Q6PGF7	Exoc8	0.43	-1.21	0.0097	24.15628142	2	12	12	81.0	Exocyst complex component 8	Mus musculus
Q9EQZ6	Rapgef4,Cgef2,Epac2	0.43	-1.21	6E-05	17.02951353	4	27	34	115.5	Rap guanine nucleotide exchange factor 4	Mus musculus
Q9R1T4	Sept6,Kiaa0128	0.43	-1.23	2E-09	9.660786628	3	31	33	49.6	Septin-6	Mus musculus
Q6PEV3	Wipf2,Wire	0.43	-1.23	5E-10	8.202605005	4	27	28	46.3	WAS/WASL-interacting protein family member 2	Mus musculus
P43024	Cox6a1,Cox6al	0.42	-1.24	9E-18	7.727212811	7	75	85	12.4	Cytochrome c oxidase subunit 6A1, mitochondrial	Mus musculus
Q9D8N0	Eef1g	0.42	-1.24	0.0156	27.39366122	2	13	15	50.1	Elongation factor 1-gamma	Mus musculus
Q9CQ69	Uqcrq	0.42	-1.24	1E-20	5.470435652	8	54	62	9.8	Cytochrome b-c1 complex subunit 8	Mus musculus
Q80Y56	Zfyve20	0.42	-1.25	0.0248	20.35215801	1	6	6	88.5	Rabenosyn-5	Mus musculus
Q9D0M3	Cyc1	0.42	-1.26	0.0009	18.53183631	2	15	16	35.3	Cytochrome c1, heme protein, mitochondrial	Mus musculus
Q9WTT4	Atp6v1g2,Atp6g2,Ng38	0.42	-1.26	0.003	13.15890756	1	7	7	13.7	V-type proton ATPase subunit G 2	Mus musculus
Q8BZ98	Dnm3,Kiaa0820	0.42	-1.26	0.0051	25.01647902	3	20	27	97.2	Dynamin-3	Mus musculus
Q9JLZ3	Auh	0.42	-1.26	0.0003	17.50185119	2	19	19	33.4	Methylglutaconyl-CoA hydratase, mitochondrial	Mus musculus
Q6ZQ38	Cand1,D10Ertd516e,Kiaa0829	0.41	-1.29	0.0099	17.99685752	1	7	7	136.3	Cullin-associated NEDD8-dissociated protein 1	Mus musculus
P28663	Napb,Snapb	0.40	-1.31	0.0112	20.85452128	1	8	8	33.6	Beta-soluble NSF attachment protein	Mus musculus
Q9Z2I8	Suclg2	0.40	-1.32	0.0494	28.91655619	1	7	8	46.8	Succinate--CoA ligase [GDP-forming] subunit beta, mitochondrial	Mus musculus
P07901	Hsp90aa1,Hsp86,Hsp86-1,Hspca	0.39	-1.35	0.0031	17.17439714	2	10	11	84.8	Heat shock protein HSP 90-alpha	Mus musculus
Q80TL4	Phf24 {ECO:0000312|MGI:MGI:2140712	0.39	-1.36	0.0008	14.62708403	2	11	12	45.2	PHD finger protein 24	Mus musculus
Q68FD5	Clta	0.39	-1.36	2E-28	6.261794065	20	132	153	191.6	Clathrin heavy chain 1	Mus musculus
P70349	Hint1,Hint,Pkci,Pkci1,Prkcnh1	0.39	-1.37	0.002	14.13317955	1	8	8	13.8	Histidine triad nucleotide-binding protein 1	Mus musculus
Q9CPX6	Atg3,Apg3l	0.38	-1.39	0.0235	19.97796924	1	6	6	35.8	Ubiquitin-like-conjugating enzyme ATG3	Mus musculus
P13647	KRT5	0.38	-1.40	2E-05	16.90380198	6	36	38	62.4	SWISS-PROT:P13647 Tax_Id=9606 Gene_Symbol=KRT5 Keratin, type II cytoskeletal 5	Homo sapiens
P08779	KRT16,KRT16A	0.37	-1.42	0.0097	28.77991481	3	24	26	51.3	SWISS-PROT:P08779 Tax_Id=9606 Gene_Symbol=KRT16 Keratin, type I cytoskeletal 16	Homo sapiens
P52503	Ndufs6,Ip13	0.37	-1.42	5E-05	16.33401252	2	23	24	13.0	NADH dehydrogenase [ubiquinone] iron-sulfur protein 6, mitochondrial	Mus musculus
Q61782	Cep131,Az1,Azi,Azi1	0.37	-1.43	0.0241	33.53181153	1	23	25	10.7	TREMBL:Q61782 Tax_Id=10090 Gene_Symbol=Krt14 Type I epidermal keratin (Fragment)	Mus musculus
P50518	Atp6v1e1,Atp6e,Atp6e2	0.37	-1.44	0.0052	25.08634666	4	20	24	26.2	V-type proton ATPase subunit E 1	Mus musculus
P56393	Cox7b	0.37	-1.45	0.0131	19.40294439	1	7	7	9.0	Cytochrome c oxidase subunit 7B, mitochondrial	Mus musculus
P28656	Napl1l,Nrp	0.37	-1.45	0.0037	16.08962706	1	8	8	45.3	Nucleosome assembly protein 1-like 1	Mus musculus

Q99JI4	Psmd6	0.36	-1.47	0.001	12.16217157	1	8	8	45.5	26S proteasome non-ATPase regulatory subunit 6	Mus musculus
Q04447	Ckb,Ckbb	0.36	-1.49	1E-06	14.70142888	4	37	38	42.7	Creatine kinase B-type	Mus musculus
Q8R1Q8	Dync1li1,Dncli1,Dnclic1	0.35	-1.52	3E-27	6.316369756	17	122	141	56.6	Cytoplasmic dynein 1 light intermediate chain 1	Mus musculus
P16125	Ldhb,Ldh-2,Ldh2	0.34	-1.54	0.0003	19.82509339	5	28	30	36.6	L-lactate dehydrogenase B chain	Mus musculus
P19536	Cox5b	0.34	-1.54	0.0011	18.94425009	2	15	17	13.8	Cytochrome c oxidase subunit 5B, mitochondrial	Mus musculus
P00405	Mtco2,COII,mt-Co2	0.34	-1.56	0.034	25.69423741	1	7	7	26.0	RecName: Full=Cytochrome c oxidase subunit 2; AltName: Full=Cytochrome c oxidase polypeptide II	Mus musculus
Q9DB77	Uqcrc2	0.33	-1.59	2E-32	4.604020521	12	92	103	48.2	Cytochrome b-c1 complex subunit 2, mitochondrial	Mus musculus
Q9QZ39	St6galnac1,Siat7a	0.33	-1.60	0.0139	16.63935763	1	6	8	60.7	Alpha-N-acetylgalactosaminide alpha-2,6-sialyltransferase 1	Mus musculus
P02538	KRT6A,K6A,KRT6D	0.32	-1.62	0.0085	25.14314213	2	14	15	60.0	SWISS-PROT:P02538 Tax_Id=9606 Gene_Symbol=KRT6A Keratin, type II cytoskeletal 6A	Homo sapiens
Q9ERS2	Ndufa13,Grim19	0.32	-1.65	0.0001	8.36774246	1	8	8	16.9	NADH dehydrogenase [ubiquinone] 1 alpha subcomplex subunit 13	Mus musculus
P97494	Gclc,Glclc	0.32	-1.66	0.0158	20.48613506	1	7	7	72.6	Glutamate--cysteine ligase catalytic subunit	Mus musculus
Q9D855	Uqcrb	0.31	-1.68	0.0003	16.84214096	2	16	16	13.5	Cytochrome b-c1 complex subunit 7	Mus musculus
Q91YD6	Vill,Villp	0.30	-1.75	0.0035	10.78457924	1	6	6	96.5	Villin-like protein	Mus musculus
Q8VDD8	Wash1,Orf19,Wash	0.29	-1.79	0.0472	28.47041997	1	7	7	51.7	WASH complex subunit 1	Mus musculus
Q9CZU6	Cs	0.29	-1.81	0.0369	26.36500118	1	7	8	51.7	Citrate synthase, mitochondrial	Mus musculus
P39053	Dnm1,Dnm,Kiaa4093	0.28	-1.84	5E-49	3.93828611	17	149	175	97.8	Dynamin-1	Mus musculus
P30275	Ckmt1	0.26	-1.94	0.001	17.37702734	2	13	16	47.0	Creatine kinase U-type, mitochondrial	Mus musculus
O88935	Syn1,Syn-1	0.24	-2.03	4E-85	2.735557626	28	226	275	74.1	Synapsin-1	Mus musculus
Q14B24	Prss57,Prssl1	0.15	-2.70	0.0007	6.688053346	1	6	7	30.3	Serine protease 57	Mus musculus
P56695	Wfs1	0.00	-1000.00			2	4	4	100.6	Wolframin	Mus musculus
P21619	Lmnb2	0.00	-1000.00			3	3	3	67.3	Lamin-B2	Mus musculus
P97807	Fh,Fh1	0.00	-1000.00			1	3	3	54.4	Fumarate hydratase, mitochondrial	Mus musculus
Q8C181	Mbnl2,Kiaa4072	0.00	-1000.00			1	3	3	40.2	Muscleblind-like protein 2	Mus musculus
Q8K021	Scamp1	0.00	-1000.00			1	3	3	38.0	Secretory carrier-associated membrane protein 1	Mus musculus
Q9CPP6	Ndufa5	0.00	-1000.00			1	3	3	13.4	NADH dehydrogenase [ubiquinone] 1 alpha subcomplex subunit 5	Mus musculus

Extented Table 4. List of the Cx30 protein partners. Analysis of the changing Cx30 interactors in WT vs KD mice. In WT cells 100 proteins were enriched or unique compared to KD cells (with the following parameters: number of peptides ≥ 3, ratio ≥ 1.5 and p-value ≤ 0.05), while in Cx30 KD cells, 261 proteins were enriched or unique (log2 ratio = -1000) compared to WT cells (with the following parameters: number of peptides ≥ 3, ratio $\geq 1/1.5$ and P-value ≤ 0.05). WT and KD proteins are highlighted in red and green, respectively. Proteins from the pathway Rho-GTPase activate ROCK are indicated for WT (bold green, Myosin 14) and KD (bold red, Rock2) samples.

Supplementary Information for

Astrocytes close the critical period for visual plasticity

Jérôme Ribot[1‡], Rachel Breton[1,2,3‡#], Charles-Félix Calvo[1], Julien Moulard[1,4], Pascal Ezan[1], Jonathan Zapata[1], Kevin Samama[1], Alexis-Pierre Bemelmans[5], Valentin Sabatet[6], Florent Dingli[6], Damarys Loew[6], Chantal Milleret[1], Pierre Billuart[7], Glenn Dallérac[1£#], Nathalie Rouach[1£*]

[*]Correspondence to:
nathalie.rouach@college-de-france.fr

This PDF file includes:

Supplementary Methods

Methods

Animals. All procedures on animals were performed according to the guidelines of European Community Council Directives of 01/01/2013 (2010/63/EU) and our local animal welfare committee (Center for Interdisciplinary Research in Biology in College de France, certificate A751901, Ministère de l'Agriculture et de la Pêche). Experiments were carried out using mice of wild type (WT) C57BL/6j background, mice expressing enhanced green fluorescent protein under the astrocytic promoter aldehyde dehydrogenase 1 family member L1 (Aldh1l1-eGFP)[1] (JAX stock #026033), as well as constitutive knockout mice for Cx30 which were previously characterized[2] and an astroglial conditional knockdown mouse line for Cx30 that we generated (hGFAP-Cre-Cx30$^{fl/fl}$, named KD). Animals were group housed on a 12 h light/dark cycle. All mice were backcrossed to the C57BL/6J background. Mice of both genders and littermates were used. All efforts were made to minimize the number of animals used and their suffering.

Generation of Cx30 knockdown mice. Astroglial Cx30 knockdown mice (KD) were generated by crossing the hGFAP-cre line constitutively expressing the cre recombinase transgene driven by the human astrocytic glial fibrillary acidic protein (hGFAP) promoter[3] (JAX stock #004600) with Cx30$^{fl/fl}$ line containing cre-excisable loxP sequences in the endogenous *Gjb6* gene[2].

Primary astrocytes cultures. Primary cortical astrocyte cultures were prepared as previously described[4]. Briefly, brains were removed (either P1-P3 pups, or P19 mice) and caudal cortices (therefore enriched in visual cortex material) were dissected in cold PBS-glucose (33 mM). Meninges were carefully removed and P1-P3 cortices were mechanically dissociated with Pasteur pipette in PBS-glucose to obtain single cell suspension. For P19 animals, caudal cortices were dissected, treated with papain (0.8 mg/ml; Worthington) for 30 min at 37°C and washed, then mechanically dissociated in PBS containing 5% FCS, 0.3% glucose and 5mM HEPES to obtain a single cell suspension. These dissociated single cell preparations were transduced with a HIV-1-derived lentivirus vector expressing GFP under the control of the PGK ubiquitous promoter (LV-PGK-GFP). Lentiviral particles were produced by transient transfection of HEK-293T cells with a three plasmids system and vector titers were quantified using an ELISA assay of p24 antigen (Gentaur, France), both as previously described[5]. Infection was performed in DMEM containing 5% SVF, 100ng of viral particles were added to 10^6 cells for 3 hours at 37°C. The suspension of infected cells was then directly seeded on polyornithine-coated glass coverslips or petri dishes (0.1 mg/ml) in DMEM containing 10% heat-inactivated FCS, 100 U/ml penicillin/streptomycin (GIBCO) and incubated at 37°C, 5% CO_2. 24 hours after transduction, the medium was replaced. After one week, once cells have reached confluency, 1 µM of cytosine-beta-D-arabinofuranoside was added to the cell culture for 2 days, to eliminate proliferating microglial cells. Medium was then changed every 3 days and astrocytes were used after 10 days in culture (10DIV). For immunocytochemistry, cells were fixed with 4% PFA and washed twice in PBS before proceeding with immunostaining. For intracerebral injection, the culture was washed with PBS, then incubated with trypsin 0.25 EDTA% (Invitrogen) for

5 to 10 min at 37°C. The harvested cells were collected in fresh DMEM 5% SVF and incubated for 2 hours at 37°C, to allow cell recovery.

Recombinant adeno-associated virus (rAAV) generation. For rAAV *in vivo* gene transfer, a transgene composed of GFP cDNA was placed under the control of a GFAP-specific promoter in a rAAV shuttle plasmid containing the inverted terminal repeats (ITR) of AAV2 (AAV-GFAP-GFP). Pseudotyped serotype 9 rAAV particles were produced by transient co-transfection of HEK-293T cells, as previously described[6]. Viral titers were determined by quantitative PCR amplification of the ITR on DNase-resistant particles and expressed as vector genome per ml (vg/ml).

Stereotaxic intracerebral injections. Animals were anaesthetized i.p. with a mix of ketamine (95mg/kg) and xylazine (12mg/kg) in 0.9 % NaCl and fitted into a stereotaxic frame (David Kopf Instruments). For cells injection, a 2µl-gauge Hamilton syringe adapted to KDS100 pump (Kd Scientific) was linked to a glass capillary (Harvard apparatus, 30-0041) that was surgically implanted in the right visual cortex area with the following coordinates to the Lambda: antero- posterior 0, medio-lateral + 2.8 and dorso-ventral - 0.5 mm. A maximum of 1.5µl of cell suspension (20 x10^4 cells) in DMEM containing 0.25% SVF was infused at a flow rate of 0.2 µl/min. Control animals were injected the same way with 1.5µl of medium. After the injection, the capillary was left in place for 5 min and then slowly withdrawn.
Alternatively for *in vivo* cell labeling, 1µl of rAAV2/9-GFAP-eGFP (diluted in PBS at a concentration of 1x10^{10} vg/µl) was unilaterally injected in the right visual cortex at the rate of 0.2µl/min using the same coordinates from Bregma mentioned above. The injection was performed using 29-gauge blunt-tip needle connected to 2µl Hamilton syringe and the injection rate was controlled by syringe pump (KD Scientific). After the injection, the needle was left in place for 5 min and then slowly withdrawn. Following surgery, mice were allowed to recover from anesthesia on a heating pad and monitored for the next 24h.

Gene Ontogy and enrichment analyzes of transcriptomic data. Comparing microarray data from P30 to P7 astrocytes (GEO# : GSE9566/plateform# : GPL1261) using Geo2R analyzes (https://www.ncbi.nlm.nih.gov/geo/info/geo2r.html)[7] allowed to identify differentially expressed genes between the two stages. Using a cut-off of 5 fold-change, about 200 up and down-regulated genes were analyzed for enrichment using their Gene Ontology assignment (GOtermFinder: https://go.princeton.edu/cgi-bin/GOTermFinder?). Process and Component GO options were selected respectively for the down and up DEG groups. Finally GO results were Visualized using ReViGO (http://revigo.irb.hr/).

Antibodies, immunohistochemistry and immunoblotting. All the antibodies used in this study are commercially available and have been validated in previous studies, as reported by the suppliers. The following primary antibodies were used: Cx30 rabbit polyclonal (1:500, 71-2200, Zymed), Cx43 mouse monoclonal (1:500, 610061 BD Biosciences), GFAP mouse monoclonal (1:500, G3893, Sigma-Aldrich), chick anti GFP (1:500, AB13970, Abcam), Parvalbumin mouse monoclonal (1:500, 235, SWANT), MMP9 rabbit (1:500, 3852, cell signaling), anti-active RhoA mouse monoclonal (1:500, 26904, NewEast Biosciences),

Lectin from Wisteria Floribunda, biotin conjugate (1:500, L1516-2MG, Sigma-Aldrich). The following fluorescent dye-conjugated secondary antibodies were used in appropriate combinations: goat anti-mouse IgG conjugated to Alexa 555 (1:2000, A-21424, Thermo Fisher), goat anti-rabbit IgG conjugated to Alexa 647 (1:2000, A-21245 Thermo Fisher). goat anti-chicken Ig conjugated to Alexa 488 (1:2000, A-11039, Thermo Fisher), Streptavidin Alexa fluor 488 (1:2000, S11223, Molecular Probes).

Immunohistochemistry and quantifications were performed as follows. Briefly, animals anesthetized with lethal dose of Dolethal (150µl /10g), were perfused by intracardiac with PBS first and 2% paraformaldehyde (PFA). The brains were carefully removed for an overnight post-fixation in the same fixative, followed by transfer in 30% sucrose for cryoprotection. Brain coronal microtome sections (40µm thick) were collected in PBS and pre-incubated 1 h with PBS-1% gelatin in the presence of 0.25% Triton-X100 (PGT). Brain sections were then stained overnight at 4°C with primary antibodies and washed in PGT three times. Appropriate secondary antibodies with DAPI (1:200, D9564, Sigma-Aldrich) were finally applied for 2 hours at room temperature. After several washes in PBS, brain slices were mounted in Fluoromount (Clinisciences) and examined with an inverted confocal laser-scanning microscope (Confocal Leica SP5 inverted). Stacks of consecutive confocal images taken with a 63x objective at 600-1000 nm intervals were acquired sequentially with two lasers (argon 488 nm and helium/neon 543 nm or 647 nm) and Z projections were reconstructed using image J software. Alternatively, primary astrocyte cultures were fixed at room temperature with 2% paraformaldehyde for 10 min, washed twice with PBS and incubated 1h with 5% non-immune goat serum (Zymed) in the presence of 0.25% Triton-X100 before proceeding as described above.

Quantifications of RhoA-GTP, WFA, MMP9, and Cx30 expression were performed with ImageJ software. WFA integrated density was determined using histogram-based thresholding method specifically around PV interneurons. RhoA-GTP and MMP9 fluorescence were evaluated by measuring the global mean intensity or the integrated density, respectively. The integrated density of Cx30 was quantified specifically in astrocytes labeled with GFP following infection with rAAV2/9-GFAP-eGFP, as described above. For the quantification of WFA, Aldh1l1 and Cx30 staining across cortical layers, confocal image stacks were acquired on four to five brain sections from each animal. Regions of interest (200 x 630µm) were randomly defined in V1 and gray values were averaged along the transversal axis (bin 1.5µm). Western blotting and quantification were performed as previously described[8]. Shortly, cells were collected with a folded pipette tip (200µl) in a small volume of PBS containing protease inhibitor cocktail (Euromedex), phosphatase inhibitors (Beta-glycerophosphate, 10 mM) and orthovanadate (1 mM), to which Laemmli 5X buffer was added. Alternatively, visual cortex samples were isolated from acute slices of 400µm cut in cold ACSF 1X. The same protocol was applied for visual cortex tissue using SDS 2% instead of PBS. Samples were sonicated, boiled 5 min and loaded on 4-12% polyacrylamide gels. Proteins were separated by electrophoresis and transferred onto nitrocellulose membranes. Membranes were saturated with 5% fat-free dried milk in triphosphate buffer solution and incubated overnight at 4°C with primary antibodies. They were then washed and exposed to HRP-conjugated secondary antibodies: goat anti rabbit IgG (1:2500, CSA2115 Clinisciences), goat anti-mouse IgG (1:2500,

CSA2108). The HRP-conjugated primary anti-GAPDH antibody (1:10,000, G9295 Sigma-Aldrich) was used as loading control. Specific signals were revealed with the chemiluminescence detection kit (Western Lightning plus-ECL, NEL103E001EA, Perkin Elmer). Semi-quantitative densitometric analysis was performed after scanning the bands with the image J software.

Proteomics and Mass Spectrometry Analysis.

Sample Preparation. Visual cortices of WT and Cx30KD mice were dissected from acute slices of 400 µm cut in cold ACSF 1X with a vibratome (Leica VT1200S). Samples were prepared in a lysis buffer containing 0.32M sucrose, 5 mM HEPES, 10 mM $MgCl_2$ and complete EDTA free, and centrifuged (8 min at 1700 g) at 4°C. The supernatant was incubated overnight with lectin from Wisteria Floribunda Agglutinin, biotin conjugate (1:500, L1516-2MG, Sigma-Aldrich) and anti-Cx30 biotinylated (using anti-Cx30 rabbit polyclonal 71-2200, Zymed and Biotinylation kit/Biotin conjugation kit ab201795, abcam) or - coupled with streptavidin beads (Immunoprecipitation Kit - Dynabeads Protein G, 10007D, Invitrogen). Then, the beads were washed with lysis buffer before mass spectrometry analysis. Two additional washes in 100 µL of ABC buffer (25 mM NH4HCO3) were performed keeping the beads in the magnet and with no incubation. Finally, beads were resuspended in 100 µl of ABC buffer and digested by adding 0.20 µg of trypsine/LysC (Promega) for 1 hour at 37 °C. Samples were then loaded onto homemade Tips packed with Empore™ C18 Extraction Disks (3M™ Discs 2215) for desalting. Peptides were eluted using 40/60 MeCN/H2O + 0.1% formic acid and vacuum concentrated to dryness.

LC-MS/MS Analysis. For the biotinylated WFA lectine pull down, liquid chromatography (LC) was performed with an RSLCnano system (Ultimate 3000, Thermo Scientific) coupled online to a Q Exactive HF-X with a Nanospay Flex ion source (Thermo Scientific). Peptides were first trapped on a C18 column (75 µm inner diameter × 2 cm; nanoViper Acclaim PepMapTM 100, Thermo Scientific) with buffer A (2/98 MeCN/H2O in 0.1% formic acid) at a flow rate of 2.5 µL/min over 4 min. Separation was then performed on a 50 cm x 75 µm C18 column (nanoViper Acclaim PepMapTM RSLC, 2 µm, 100Å, Thermo Scientific) regulated to a temperature of 50°C with a linear gradient of 2% to 30% buffer B (100% MeCN in 0.1% formic acid) at a flow rate of 300 nL/min over 91 min. MS full scans were performed in the ultrahigh-field Orbitrap mass analyzer in ranges m/z 375-1500 with a resolution of 120 000 at m/z 200. The top 20 intense ions were subjected to Orbitrap for further fragmentation via high energy collision dissociation (HCD) activation and a resolution of 15 000 with the AGC target set to 10^5 ions. We selected ions with charge state from 2+ to 6+ for screening. Normalized collision energy (NCE) was set at 27 and the dynamic exclusion of 40s.

For the Cx30 pull down, LC was performed as previously with an RSLCnano system (same trap column, column and buffers), coupled online to an Orbitrap Exploris 480 mass spectrometer (Thermo Scientific). Peptides were trapped onto a C18 column with buffer A at a flow rate of 3.0 µL/min over 4 min. Separation was performed at a temperature of 40°C with a linear gradient of 3% to 29% buffer B at a flow rate of 300 nL/min over 91 min. MS full scans were performed in the ultrahigh-field Orbitrap mass analyzer in ranges *m/z* 375-

1500 with a resolution of 120 000 at *m/z* 200. The top 20 most intense ions were subjected to Orbitrap for further fragmentation via high energy collision dissociation (HCD) activation and a resolution of 15 000 with the AGC target set to 100%. We selected ions with charge state from 2+ to 6+ for screening. Normalized collision energy (NCE) was set at 30 and the dynamic exclusion of 40s.

Data analysis. For identification, the data were searched against the Mus Musculus Swiss-Prot database (UP 000000589 containing 17038 sequences) and also a databank of the common contaminants containing 245 sequences for the Cx30 pull downs using Sequest–HT through proteome discoverer (version 2.2). Enzyme specificity was set to trypsin and a maximum of two-missed cleavage sites were allowed. Oxidized methionine and N-terminal acetylation were set as variable modifications. Maximum allowed mass deviation was set to 10 ppm for monoisotopic precursor ions and 0.02 Da for MS/MS peaks. The resulting files were further processed using myProMS[9] v3.5 (https://github.com/bioinfo-pf-curie/myproms). FDR calculation used Percolator[10] and was set to 1% at the peptide level for the whole study. The label free quantification was performed by peptide Extracted Ion Chromatograms (XICs) computed with MassChroQ version 2.2.1[11]. For protein quantification, XICs from proteotypic peptides shared between compared conditions (TopN matching) and missed cleavages of peptides were used. Median and scale normalization was applied on the total signal to correct the XICs for each biological replicate. To estimate the significance of the change in protein abundance, a linear model (adjusted on peptides and biological replicates) based on two-tailed T-tests was performed and P-values were adjusted with a Benjamini-Hochberg FDR.
Proteins from the biotinylated WFA lectine pull down with at least three total peptides in all replicates (n=3), a 1.5-fold enrichment and an adjusted P-value < 0.05 were considered significantly enriched in sample comparison. Unique proteins were considered with at least three total peptides in all replicates. Protein selected were further analyzed with Reactome pathway analysis (https://reactome.org/PathwayBrowser/#TOOL=AT,[12]). Considering the lack of functional annotation in Mus Musculus, protein pathways were retrieved from the mapping of selected proteins to Homo Sapiens.

Electroretinography. The changes in potentials induced by light flashes in the retinal tissue were recorded with a Siem Medical ERG system (Nîmes, France). The active electrode (a gold loop) was placed on the cornea, while reference and ground electrodes were placed subcutaneously above the skull and in the tail, respectively. Mice were dark-adapted prior to the experiment, being housed in a dark-room on the evening prior to the recordings. On the following day, mice were handled under dim red light to maintain dark adaptation. After pupil dilatation with a drop of atropine and anesthesia with an intraperitoneal injection of a mixture of ketamine + medetomidine hydrochloride, the mice were placed on a mobile platform with a heating pad, to maintain body temperature. Ophthalmic gel was applied on both eyes, to keep the cornea moist and favor electric contact with the active electrode. After placement of the electrodes, the platform was moved forward so that the head of the mice was inside of the Ganzfeld delivering the flashes. After a series of flashes of increasing intensity (from 20 mCd.s.m-2 to 10 Cd. s.m-2), a background light of 25 Cd.m-2 was applied for 15 minutes, to saturate the rod photoreceptors and light adapt the cones, and

flashes of 1 and 10 Cd.s.m-2 were applied. The cone system was further tested using flicker stimuli delivered at 2, 10, 15 and 20 Hz, with the same 25 Cd.m-2 background light.

Monocular deprivation. For monocular deprivation, mice were anesthetized i.p. with a mix of ketamine (95mg/kg) and xylazine (12mg/kg) in 0.9 % NaCl. The area surrounding the eye to be sutured was trimmed and wiped with 70% ethanol. Two mattress sutures were then placed and animals were checked daily to ensure sutures remained intact.

Intrinsic optical imaging.

Surgery. Mice were anesthetized with urethane (1.2 g/kg, i.p.) and sedated with chlorprothixene (8 mg/kg, i.m.). Atropine (0.1 mg/kg) and dexamethasone (2 mg/kg) were injected subcutaneously. The animals were placed in a stereotaxic apparatus and the body temperature was maintained at 37°C. In some cases, a craniotomy was made over the visual cortex. The exposed area was then covered by agarose (2.5%) and a glass coverslip. In other cases, the skull was left intact and intrinsic signals were recorded directly though the skull. No difference was found between the two methods.

Visual stimulation and optical imaging recording. Visual cortical responses were recorded using imaging methods based on Fourier transform following periodic stimulation[13,14]. Visual stimuli were presented on a high refresh rate monitor placed 20 cm in front of the mouse. Stimulation consisted of a horizontal bar drifting downwards periodically at a period of 8 s in the binocular visual field of the recorded hemisphere (from +5° ipsilateral to +15° contralateral). Each eye was stimulated 5 times in alternance for 2 to 4 minutes. Intrinsic signals were recorded using a 1M60 CCD camera (Dalsa) with a 135x50 mm tandem lens (Nikon) configuration. After acquisition of the surface vascular pattern, the camera was focused 400 µm deeper. Intrinsic signals were acquired with a 700 nm illumination wavelength and frames stored at a rate of 10 Hz, after a 2x2 pixels spatial binning.

Data analysis. Retinotopic maps for each eye were computed offline. Prior to Fourier transform, the generalized indicator function[15] was applied to remove slow varying components independent of the stimulation. Retinotopic maps were calculated from the phase and magnitude components of the signal at the frequency of stimulation. For each eye, the five activity maps were averaged, filtered with a Gaussian kernel low-pass filter (3 pixels s.d.) and set with a cut-off threshold at 50% of the maximum response. This allowed defining the binocular zone as the intersection between the response regions of each eye. For each of the 5 repetitions, an OD value at each pixel in the binocular zone was then defined as (C-I)/(C+I), calculated from the response amplitude from the contralateral (C) eye and the ipsilateral (I) eyes. OD values ranged from -1 to 1, with negative values representing an ipsilateral bias, and positive values a contralateral bias. From these 5 OD maps, the OD index was then computed as the average of the OD values in the binocular zone. The OD indexes of one animal were averaged for statistical comparisons between ages, strains and conditions.

Slices preparation and electrophysiology. After rapid extraction of the brain, coronal slices (400 µm) containing the visual cortex were cut by mean of a vibratome (Leica VT1200S) and allowed to recover for a minimum of 45 min at 30°C in a submerged chamber containing ACSF before recording. Slices were individually transferred in a recording chamber placed under a microscope (Slicescope SSPro1000) and continuously perfused (2 mL/min) with aCSF composed of (in mM): 119 NaCl, 2.5 KCl, 2.5 $CaCl_2$, 1.3 $MgSO_4$, 1 NaH_2PO_4, 26.2 $NaHCO_3$ and 11 glucose. For recording of spontaneous synaptic activity, layer 4 pyramidal neurons from the primary visual cortex were recorded by whole-cell patch clamp using 3-6 MΩ glass pipettes filled with (in mM): 144 potassium gluconate, 1 $MgCl_2$,10 HEPES, 0.5 EGTA (pH 7.4, 280 mOsm). Spontaneous excitatory or inhibitory postsynaptic potentials (sEPSCs or sIPSCs) were identified as inward and ourward currents, respectively. Excitation-inhibition (E-I) balance was determined as described previously[16,17]. Briefly, electrical stimulations (10-100 µA, 0.2 ms, 0.05 Hz) were applied in layer 2 of the visual cortex using a 1 MΩ monopolar glass pipette filled with aCSF. Under voltage-clamp, 5 trials were repeated for 5 holding potentials (-70mV to -50mV). Data were analysed off-line with Elphy (NeuroPSI-CNRS, Gif-sur-Yvette, France). The E-I balance determination is based on the continuous measurement of conductance dynamics during the full-time course of the stimulus-evoked synaptic response. Briefly, we performed post-hoc decomposition of postsynaptic current waveforms in excitatory and inhibitory conductances together with continuous estimation of the apparent reversal potential of the composite responses. This allows a somatic measurement of the E-I balance after dendritic integration of incoming excitation and inhibition[17]. In order to extract the excitatory and inhibitory conductance changes from the evoked synaptic currents, the neuron is considered as the point-conductance model of a single-compartment cell, described by the following general membrane equation:

$$Cm\,\frac{dVm(t)}{dt} = -gleak(Vm(t) - Eleak) - gE(t)(Vm(t) - Eexc) - gI(t)(Vm(t) - Einh) + Iinj$$

where C_m denotes the membrane capacitance, I_{inj} the injected current, g_{leak} the leak conductance and E_{leak} the leak reversal potential. gE(t) and gI(t) are the excitatory and inhibitory conductances, with respective reversal potentials E_{exc} and E_{inh}. Evoked synaptic currents were measured and averaged for 5 holding potentials. IV curves were then calculated at all time points of the response. In IV curves for every possible delay (t), the value of holding potential (V_h) was corrected (V_{hc}) from the ohmic drop due to leakage current through the access resistance ($V_{hc}(t) = V_h(t) – I(t) \times R_s$). An average estimate of the input conductance waveform of the cell was calculated from the best linear fit (mean least square criterion) of the IV curve for each delay (t) following the stimulation onset. Only cells showing a Pearson correlation coefficient for the IV linear regression higher than 0.95 between -90 and -40 mV were considered for calculation of the conductance change in the recorded pyramidal neuron, using the slope of the regression line. The synaptically-evoked global conductance term ($g_T(t)$) was then measured by subtracting the resting conductance observed in the absence of stimulation (on a time window of 100 ms before electrical stimulation) from the input total conductance. The synaptic reversal potential of the synaptic conductance ($E_{syn}(t)$) was taken as the voltage of the intersection between the IV curve

during the synaptic response and the IV curve at rest. Assuming that the evoked somatic conductance change reflects the composite synaptic input reaching the soma, $E_{syn}(t)$ characterizes the stimulation-locked dynamics of the balance between excitation and inhibition. The global synaptic conductance ($g_T(t)$) was further decomposed into two conductance components ($g_E(t)$ and $g_I(t)$) corresponding to the activation of excitatory and inhibitory synapses respectively, each associated with known and fixed reversal potentials: 0 mV for excitatory (E_{exc}) and -80 mV for inhibitory conductance (E_{inh}). Under our experimental conditions, $E_{syn}(t)$ took any intermediate values between E_{exc} (0 mV) and E_{inh} (-80 mV) in such a way that the mathematical conditions of the simplification used to calculate $g_I(t)$ and $g_E(t)$ were fulfilled. For each component, excitatory and inhibitory, we calculated the conductance change as the mean averaged over a time window of 200 ms. The contribution of each component was expressed by the ratio of its integral value to that of global conductance change.

Fasudil treatment. Fasudil hydrochloride (F4660, LC laboratories, Boston, MA, USA) was prepared by diluting 5 mL of solution stock Fasudil 10X (1g Fasudil hydrochloride for 150 mL H2O) in 50 mL of water. The treatment was given for 4 weeks (from P20 to P50) in drinking water (ad libitum; around 3 mg/day/mouse). Drinking bottles were wrapped in aluminium to avoid phototoxicity and replaced every 2 days[18].

Statistical analysis. All data are presented as mean ± standard error of the mean (SEM) and n represent the number of independent replicates. All statistical analyses were performed with GraphPad Prism (GraphPad sofware, USA). Prior statistical comparison, the normality of the distributions were studied and appropriate parametric or nonparametric tests were used. Stastistical significance between two groups was evaluated with a two-tailed t-test or Mann-Whitney test. Concerning within-group comparisons, statistical significance was determined with an ANOVA (One- or two-way) or a Kruskal-Wallis followed by post hoc tests (Tukey or Sidak post-hoc tests for the ANOVA; Dunn post-hoc test for Kruskal-Wallis). Appropriate sample sizes were based on best practices in the literature for each method as well as on ethical standards to minimize numbers of animals for experiments.

Data availability. We confirm that all relevant data are included in the paper and/or its supplementary information files. The mass spectrometry proteomics data have been deposited to the ProteomeXchange Consortium via the PRIDE[19] partner repository with the dataset identifier PXD020448 (Username: reviewer87927@ebi.ac.uk, Password: nmA5W4eW).

References

1 Tsai, H. H. *et al.* Regional astrocyte allocation regulates CNS synaptogenesis and repair. *Science* **337**, 358-362, doi:10.1126/science.1222381 (2012).
2 Boulay, A. C. *et al.* Hearing is normal without connexin30. *J Neurosci* **33**, 430-434, doi:10.1523/JNEUROSCI.4240-12.2013 (2013).
3 Zhuo, L. *et al.* hGFAP-cre transgenic mice for manipulation of glial and neuronal function in vivo. *Genesis* **31**, 85-94, doi:10.1002/gene.10008 (2001).
4 Rouach, N., Calvo, C. F., Glowinski, J. & Giaume, C. Brain macrophages inhibit gap junctional communication and downregulate connexin 43 expression in cultured

astrocytes. *Eur J Neurosci* **15**, 403-407, doi:10.1046/j.0953-816x.2001.01868.x (2002).

5 Qamar Saeed, M. *et al.* Comparison Between Several Integrase-defective Lentiviral Vectors Reveals Increased Integration of an HIV Vector Bearing a D167H Mutant. *Mol Ther Nucleic Acids* **3**, e213, doi:10.1038/mtna.2014.65 (2014).

6 Berger, A. *et al.* Repair of rhodopsin mRNA by spliceosome-mediated RNA trans-splicing: a new approach for autosomal dominant retinitis pigmentosa. *Mol Ther* **23**, 918-930, doi:10.1038/mt.2015.11 (2015).

7 Cahoy, J. D. *et al.* A transcriptome database for astrocytes, neurons, and oligodendrocytes: a new resource for understanding brain development and function. *J Neurosci* **28**, 264-278, doi:10.1523/JNEUROSCI.4178-07.2008 (2008).

8 Pillet, L. E. *et al.* The intellectual disability protein Oligophrenin-1 controls astrocyte morphology and migration. *Glia* **68**, 1729-1742, doi:10.1002/glia.23801 (2020).

9 Poullet, P., Carpentier, S. & Barillot, E. myProMS, a web server for management and validation of mass spectrometry-based proteomic data. *Proteomics* **7**, 2553-2556, doi:10.1002/pmic.200600784 (2007).

10 The, M., MacCoss, M. J., Noble, W. S. & Kall, L. Fast and Accurate Protein False Discovery Rates on Large-Scale Proteomics Data Sets with Percolator 3.0. *J Am Soc Mass Spectrom* **27**, 1719-1727, doi:10.1007/s13361-016-1460-7 (2016).

11 Valot, B., Langella, O., Nano, E. & Zivy, M. MassChroQ: a versatile tool for mass spectrometry quantification. *Proteomics* **11**, 3572-3577, doi:10.1002/pmic.201100120 (2011).

12 Jassal, B. *et al.* The reactome pathway knowledgebase. *Nucleic Acids Res* **48**, D498-D503, doi:10.1093/nar/gkz1031 (2020).

13 Cang, J. *et al.* Development of precise maps in visual cortex requires patterned spontaneous activity in the retina. *Neuron* **48**, 797-809, doi:10.1016/j.neuron.2005.09.015 (2005).

14 Kalatsky, V. A. & Stryker, M. P. New paradigm for optical imaging: temporally encoded maps of intrinsic signal. *Neuron* **38**, 529-545, doi:10.1016/s0896-6273(03)00286-1 (2003).

15 Yokoo, T., Knight, B. W. & Sirovich, L. An optimization approach to signal extraction from noisy multivariate data. *Neuroimage* **14**, 1309-1326, doi:10.1006/nimg.2001.0950 (2001).

16 Meunier, C. N. *et al.* D-Serine and Glycine Differentially Control Neurotransmission during Visual Cortex Critical Period. *PLoS One* **11**, e0151233, doi:10.1371/journal.pone.0151233 (2016).

17 Monier, C., Fournier, J. & Fregnac, Y. In vitro and in vivo measures of evoked excitatory and inhibitory conductance dynamics in sensory cortices. *J Neurosci Methods* **169**, 323-365, doi:10.1016/j.jneumeth.2007.11.008 (2008).

18 Meziane, H. *et al.* Fasudil treatment in adult reverses behavioural changes and brain ventricular enlargement in Oligophrenin-1 mouse model of intellectual disability. *Hum Mol Genet* **25**, 2314-2323, doi:10.1093/hmg/ddw102 (2016).

19 Perez-Riverol, Y. *et al.* The PRIDE database and related tools and resources in 2019: improving support for quantification data. *Nucleic Acids Res* **47**, D442-D450, doi:10.1093/nar/gky1106 (2019).